Three in One: In Vitro and In Vivo Evaluation of Anticancer Activity of a Theranostic Agent that Combines Magnetic Resonance Imaging, Optical Bioimaging, and Photodynamic Therapy Capabilities

Sarah Boumati, Angélique Sour, Valérie Heitz, Johanne Seguin, Gautier Beitz, Yusuke Kaga, Marta Jakubaszek, Johannes Karges, Gilles Gasser, Nathalie Mignet, et al.

Three in One: Anti Cancer Activity *in vitro* and *in vivo* Evaluation of a Theranostic Agent that Combines Magnetic Resonance Imaging, Optical Bioimaging and Photodynamic Therapy Capabilities

*Sarah BOUMATI[1], Angélique SOUR[2], Valérie HEITZ[2], Johanne SEGUIN[4], Gautier BEITZ[1], Yusuke KAGA[1], Marta JAKUBASZEK[3], Johannes KARGES[3], Gilles GASSER[3], Nathalie MIGNET[4], Bich-thuy DOAN[1]**

1. Université PSL Chimie ParisTech, CNRS, Institute of Chemistry for Life and Health Sciences (I-CLeHS), SEISAD, 75005 Paris, France
2. Université of Strasbourg, Institut de Chimie de Strasbourg, CNRS, UMR 7177, Laboratoire LSAMM, 67070 Strasbourg, France
3. Université PSL, Chimie ParisTech, CNRS, Institute of Chemistry for Life and Health Sciences (I-CLeHS), Laboratory for Inorganic Chemical Biology, 75005 Paris, France
4. Université Paris Cité, CNRS, Inserm, Unité de Technologies Chimiques et Biologiques pour la Santé (UTCBS), 75006 Paris, France

.

KEYWORDS Bioimaging, Cancer, Gd-based Contrast Agent, Photodynamic Therapy, Photosensitizer, Theranostic Agent.

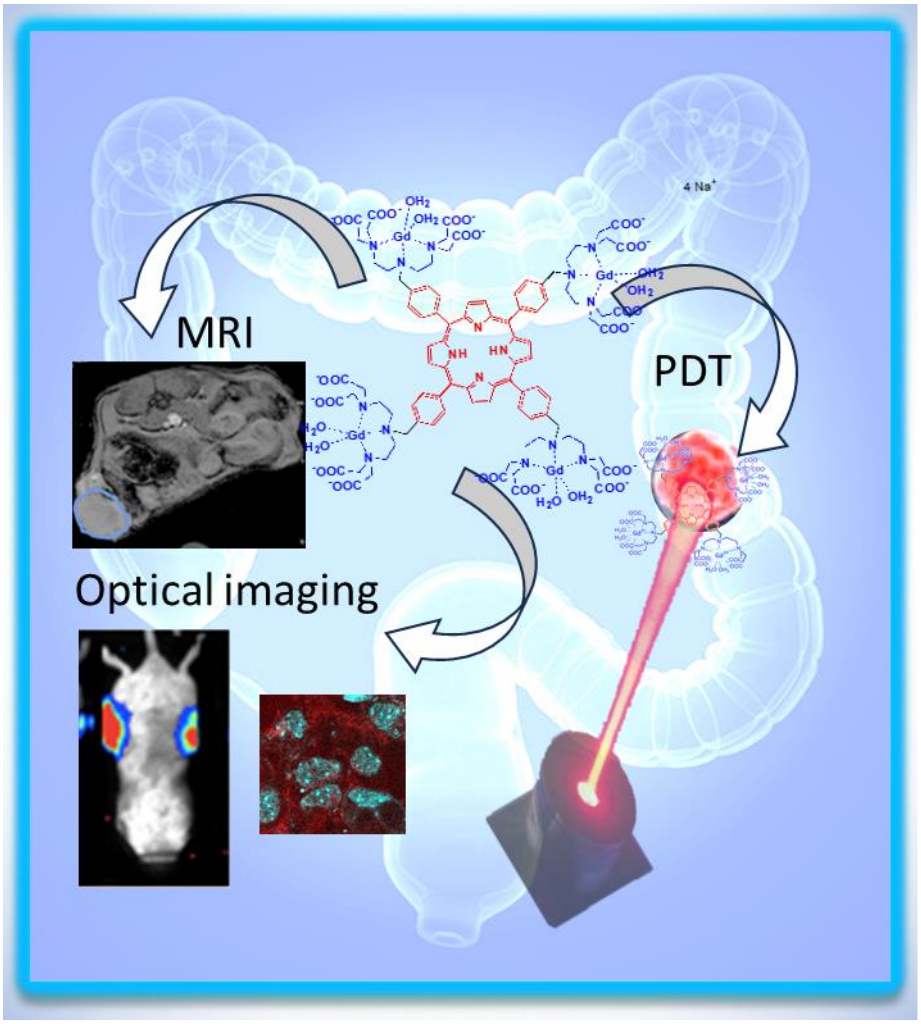

ABSTRACT Cancer treatment is a crucial area of research and development as current chemotherapeutic treatments can have severe side effects or poor outcomes. In the constant seek of new strategies that are localized, minimally invasive, and produce minimal side effects, photodynamic therapy (PDT) is an exciting therapeutic modality that is gaining attention. The use of theranostics, which combines diagnostic and therapeutic capabilities, can further improve treatment monitoring through image guidance. This study explores the potential of a theranostic agent consisting of four Gd(III) DTTA complexes (DTTA: diethylenetriamine-N, N, N'', N''-tetraacetate) grafted to a *meso*-tetraphenylporphyrin core for PDT, fluorescence and magnetic resonance imaging (MRI). The agent was first tested *in vitro* on both non-malignant TIB-75 and MRC-5 as well as tumoral CT26 and HT-29 cell lines and subsequently evaluated *in vivo* in a preclinical colorectal tumor model. Advanced MRI and optical imaging techniques were employed with engineered quantitative *in vivo* molecular imaging based on MRI dynamic acquisition sequences to track the agent's biodistribution in the body. With 3D quantitative volume computed by MRI and tumoral cells function assessed by bioluminescence imaging, we could demonstrate a significant impact of the molecular agent on tumor growth following light application. Further exhaustive histological analysis confirmed these promising results, making this theranostic agent a potential drug candidate for cancer.

1. INTRODUCTION

Increasing research efforts are dedicated towards the development of novel anticancer drugs and strategies to overcome side effects with targeted or activatable therapies. In addition to techniques commonly used in hospital, such as surgery, chemotherapy, or radiotherapy, immunotherapy and photodynamic therapy (PDT) have emerged as efficient complementary or even alternative strategies. In particular, PDT is based on the local activation of a photosensitizer (PS) by irradiation to generate reactive oxygen species (ROS)[1].

Most currently approved photosensitizers (PSs) are based on tetrapyrrolic structures (i.e., porphyrin, chlorin, phthalocyanine) which present several advantages,[2–5] such as good chemical stability, harmlessness in the absence of light, tunable absorption and emission, efficient ROS generation, as well as the possibility to use them as optical imaging agents due to their luminescence properties. Nevertheless, their usual drawbacks are poor aqueous solubility, aggregation, photobleaching, slow clearance from the body, hepatotoxicity and poor tumor cell selectivity[2]. Moreover, for *in vivo* applications, as the light tissue penetration depth is rather poor at the visible wavelengths, the application of these compounds to treat deep-seated or large tumors is limited.[6,7] Therefore, to overcome these limitations, an active work is performed in the development of new classes of PSs with an absorption towards the biological spectral window (NIR 700-900 nm). In particular, the development of a fourth generation of photosensitizers has highlighted the therapeutic potential that a single multimodal platform carrying the functions of imaging and therapy on a same scaffold named theranostics[8] could have in the detection and treatment of diseases. Such system eliminates the need to administer several agents individually, therefore allowing to follow the pharmacokinetics of the therapeutic agents together with their tracking probe. Moreover, although the porphyrin-based PSs can be detected by luminescence

imaging, there is a need to improve their design to detect them at any depth and optimize the monitoring of the PDT treatment with 3D imaging such as Magnetic Resonance Imaging (MRI).

Combining the therapeutic and diagnostic capabilities into a single agent should facilitate the detection and treatment of disease and could lead to more specific and effective agents for the management of the disease. So far, theranostic research has mainly focused on cancer[8]. Most theranostics are based on nano-sized platforms, such as inorganic nanoparticles[1,9], polymeric conjugates, liposomes and micelles[6,10]. However, water-soluble molecular agents also offer advantages as they allow easier scale-up and control of physicochemical properties. A few examples of DTPA (diethylenetriamine pentaacetate), DTTA (diethylenetriamine-N, N, N'', N''-tetraacetate) or DO3A (Tetraazacyclododecane-triacetate) Gd complexes linked to porphyrins or derivatives and porphyrazines complexed with Gd showed higher longitudinal relaxivities, in vitro cells internalisation and efficient PDT *in vitro* and *in vivo*.[11–15] Their photophysics in solution, *in vitro* evaluation and a qualitative *in vivo* biodistribution in a tumor rodent model[11,13] showed the potentiality of this MRI theranostic family of Gd complex-porphyrin conjugates for PDT. Heitz and co-workers developed DPP-ZnP-$(GdDOTA)_2$[16] and GdDOTA-ZnP-ZnP-GdDOTA[17] complexes consisting of π-extended Zn(II) porphyrin as photosentizers for PDT linked to two GdDOTA-type complexes for MRI detection. Both molecules showed high relaxivity (r1= 19.32 $mM^{-1}s^{-1}$ and 14.33 mM^{-1} s^{-1}, for DPP-ZnP-$(GdDOTA)_2$ and GdDOTA-ZnP-ZnP-GdDOTA respectively, at 20 MHz and 298 K per Gd3+ ions concentration) compared to clinical contrast agents. *In vitro* Hela cells studies of internalisation and in vitro PDT at 660 nm evidenced the potentiality of these molecules as theranostic agent. The same group[18] also described the design, synthesis and characterisation of a MRI/PDT molecular agent Porph$(GdDTTA)_4$ consisting of a

meso-tetraphenylporphyrin endowed with four Gd(III)DTTA^{-} complexes. This conjugate showed remarkably high longitudinal relaxivity in water (r_1 = 43.7 $mM^{-1}.s^{-1}$ per Gd(III) center at 20 MHz and 8.8 $mM^{-1}.s^{-1}$ at 300 MHz at 25°C) for MRI monitoring, singlet oxygen photosensitizing properties in the deep red wavelengths and good phototoxicity on Hela cells. The remarkable relaxivity properties were related to (i) the choice of GdDTTA^{-} complexes binding two inner-sphere water molecules per Gd instead of one for DTPA, DO3A and DOTA-based complexes[11–13,16,17] and (ii) short and rigid linkers used to connect the Gd complexes to the porphyrin core.[15]

Based on the promising results obtained in solution and culture cells,[18] our specific objective in this work was to evaluate the potential of the conjugate as a theranostic agent *in vivo*. We aimed to show the PDT efficacy on a murine tumor model with MR and bioluminescence imaging to monitor tumor growth.

2. EXPERIMENTAL SECTION

2.1. Reagents

All basic chemical reagents are from commercial sources and have been used without purification. Dulbecco's Modified Eagles Medium supplemented with F-12 Nutrient Mix (DMEM / F-12), Fetal Bovine Serum (FBS), Antibiotic Penicillin-Streptomycin-Glutamine (Penstrep) were purchased from Gibco, Buffered Saline Solution Dulbecco's phosphate (PBS) were purchased from Fisher Scientific (Illkirch, France), resazurin from ACROS Organics (Noisy le Grand, France) and Protoporphyrin IX from Sigma Aldrich Merck (France). Murine colon carcinoma cell line CT26, hepatocytes cell line TIB-75, human lung fibroblasts MRC-5, colon carcinoma cell line HT-29 were purchased from the American Type Culture Collection (LGC Standards, Molsheim,

France.). Primary anti-mouse CD31 (PECAM1) monoclonal antibody and secondary goat anti-rat biotinylated rat antibody (BD Biosciences, le Pont de Claix, France), streptavidin-conjugated peroxidase and 3,3-diaminobenzidine substrate DAB (Sigma Aldrich Merck, France) were used.

2.2 Spectroscopic measurements

The absorption spectra of the samples were measured with a SpectraMax M2 spectrometer (Molecular Devices, San Jose, CA, USA). The emission spectra were measured after irradiation of the sample at 510 nm in fluorescence quartz cuvettes (width 1 cm) using a pumped optical parametric oscillator NT342B Nd-YAG (Ekspla, Vilnius, Lithuania). The emission was focused, collected and directed towards a monochromator (Acton SP-2300i, Princeton Instruments). The signal was detected using a PI-Max 4 CCD camera (Princeton Instruments, Trenton, NJ, USA).[19]

2.3. Luminescence quantum yield measurements

For the determination of the luminescence quantum yield, the samples were prepared in an aqueous solution with an absorbance of the photosensitizer of 0.1 at 510 nm. The solution was irradiated at 510 nm and the emission signal was detected with the same system as described in the previous section about the spectroscopic measurements. The luminescence quantum yields were determined by comparison with the reference $[Ru(bipy)_3]Cl_2$ in water (Φ_{em}=4.2 %)[20] by applying the following formula:

$$\Phi_{em,sample} = \Phi_{em,reference} \times (F_{reference} / F_{sample}) \times (I_{sample} / I_{reference}) \times$$

$$(n_{sample} / n_{reference})^2$$

$$F = 1 - 10^{-A}$$

Φ_{em} = luminescence quantum yield, F = fraction of light absorbed, I = measured fluorescence intensities, n = refractive index of solvents, A = absorbance of the sample at irradiation wavelength.

2.4. Fluorescence lifetime measurements.

For the determination of the excited state lifetimes, the samples were prepared in an air saturated aqueous solution with an absorbance of 0.1 at 510 nm. The solution was irradiated in fluorescence quartz cuvettes (width 1 cm) at 510 nm using the same system as described in the previous section about the spectroscopic measurements. Emission spectra were measured with an increasing temporal delay. For the data analysis, the emission signal was integrated and the resulting areas plotted against the used delay.[21]

2.5 Singlet oxygen measurements - Direct evaluation

The measurement is called direct because it is based on the luminescence of the singlet oxygen formed after excitation with an appropriate wavelength. The samples were prepared in air saturated water D_20 with an absorbance of 0.2 at the irradiation wavelength (505 or 660 nm). This solution was irradiated at 505 or 660 nm. The singlet oxygen luminescence at 1270 nm was measured by recording spectra from 1100 to 1400 nm. For the data analysis, the singlet oxygen luminescence peaks at different irradiation intensities were integrated. The resulting areas were plotted against the percentage of the irradiation intensity and the slope of the linear regression calculated. The absorbance of the sample was corrected with an absorbance correction factor.[6] As references[22] for the measurement, rose bengal ($\Phi_{\text{rose bengal}}$ = 76 %) and methylene blue ($\Phi_{\text{methylene blue}}$ = 52%) were used and the singlet oxygen quantum yields were calculated using the following formula:

$\Phi_{sample} = \Phi_{reference} \times (S_{sample} / S_{reference}) \times (I_{reference} / I_{sample})$

$I = I_0 * (1 - 10^{-A})$

Φ = quantum efficiency of singlet oxygen, S = slope of the linear regression of the plot of the singlet oxygen luminescence peak areas as a function of the irradiation intensity, I = absorbance correction factor, I_0 = light intensity of the irradiation source, and A = absorbance of the sample at the irradiation wavelength.

2.6 Singlet oxygen measurements - Indirect evaluation

This method is based on monitoring of the absorption quench kinetics of a singlet oxygen scavenger. In the presence of the photosensitizer and under light irradiation, the generated singlet oxygen will oxidize the reporter molecule and significantly change its absorption properties. The samples were prepared in PBS and CH_3CN containing the compound with an absorbance of 0.1 at the irradiation wavelength (510 or 660 nm), the scavenger *N*,*N*-dimethyl-4-nitrosoaniline (RNO, 24 μM) and histidine (12 mM). Samples were irradiated on 96-well plates with a LUMOS BIO irradiator (Atlas Photonics, Fribourg, Switzerland) every minute for 10 min. The absorbance of the samples was measured during these time intervals with a SpectraMax M2 microplate reader (Molecular Devices, San Jose, CA, USA). The difference in absorbance (A_0-A) at 510 nm was calculated and plotted against the irradiation times. From the graph, the slope of the corresponding plot was calculated. The absorption of the sample was corrected with an absorption correction factor. Singlet oxygen quantum yields were calculated using the same formulas used for direct evaluation.[19]

2.7 Cell culture

Murine colon adenocarcinoma (CT26), human colon adenocarcinoma (HT-29), and murine hepatocyte (TIB-75) cells were cultured using DMEM media. Human embryonic fibroblast cells (MRC-5) were cultured using DMEM / F-12 medium with the addition of 10 % FBS and 1 % Penstrep. These cells come from the American Type Culture Collection (ATCC). They were grown and maintained in a cell culture incubator at 37 ° C with an atmosphere of 5 % CO_2. Before any experiment, the cells were subcultured three times.

2.8 Cell internalization study

A total of 1 x 10^6 cells (4 types: CT26, TIB-75, MRC-5 and HT-29) were inoculated into 24-well kneaders containing round coverslips (refraction index 0.5) and allowed to adhere overnight in the oven (5 % CO_2, 37°C). The cells were incubated with the sample (PpIX and Porph(GdDTTA)$_4$, 1 µM) for 4 hours in the incubator. After this time, the cells were washed three times with PBS and then fixed with 4 % PFA for 10 minutes at room temperature. After washing with PBS the coverslips were mounted with mounting medium containing 90 % glycerol and Hoechst 1/5000 in PBS to stain the cells nuclei.

Confocal images were taken with an LSM 880 confocal laser scanning microscope (Carl Zeiss, Cellular Imaging Platform of the Faculty of Pharmacy, Paris). The samples were detected using their one-photon luminescence properties (λex = 358-405 nm, λem = 461-650 nm) for the Hoechst and Porph(GdDTTA)$_4$ staining respectively.

2.9 Cytotoxicity

The cells are cultured to assess the cytotoxicity and phototoxicity of the compounds, here our photosensitizer Porph(GdDTTA)$_4$ and a reference one which is protoporphyrin IX (PpIX), by

measuring cell viability with the resazurin fluorometric assay. Cultured cells were seeded in triplicate in 96-well plates with a density of 4000 cells per well in 100 µL of medium.

After 24 h of cell seeding, the culture medium was removed and the cells were treated with increasing concentrations of the test compound diluted in the cell medium to a total volume of 200 µL. The cells were incubated with increasing concentrations of the test compound for 24 h (range 1 to 300 µM). After this time, the medium was replaced with fresh medium containing resazurin at a final concentration of 0.2 mg / ml. After 4 h of incubation, the amount of reduced resazurin in resorufin by the metabolically active cells was determined by excitation at 540 nm and measurement of its emission at 590 nm using a SpectraMax M2 microplate reader (Molecular Devices, San Jose, CA, USA). The obtained data were analyzed to calculate the IC50, with the GraphPad Prism software (Boston, MA, USA).

2.10 Phototoxicity

The phototoxicity was measured with the same set up for cells irradiation in the indirect singlet oxygen method measurements (section 6).

a) Determination of the maximum irradiation duration, which corresponds, to the dose of non-cytotoxic light for the cells (without product)

The 4 types of cells are maintained in culture for 24 h in 96-well plates (7 plates / cells, 4000 cells / well). For each type of cells, a plate is maintained for 1 hour at 37 ° C then returned back to the incubator, a plate left in the incubator (37 ° C, 0.5 % CO_2) and 5 other plates are irradiated for several times of 20, 30, 40, 50, and 60 min at a wavelength of 645 nm for each product used in the phototoxicity study (here Porph(GdDTTA)$_4$ and PpIX). Cell viability was determined by the resazurin test (0.2 mg/ml) after 48 incubation (37° C, 0.5% CO_2).

b) Determination of the IC_{50} in the presence of Porph(GdDTTA)$_4$ with and without irradiation for the calculation of the phototoxicity index (PI) which reflects the phototoxic potential of Porph(GdDTTA)$_4$.

The cells are kept in culture for 24 hours until monolayers form. For each chemical product tested, 6 96-well plates are then preincubated for 4 hours with 9 distinct concentrations of the photosensitizer (from 0 to 300 µM). Then, after changing the medium, three of the six plates were exposed to a dose of light determined in the first step (SI 5 figures SI 5 A and B, 20 min, using a light dose of 10 J.cm^{-2}, 8mW.cm^{-2} power) and to a wavelength corresponding to the products tested (Porph(GdDTTA)$_4$ and PpIX: 645 nm) using the LUMOS BIO led irradiator while the other three plates were kept in the dark. After 48 hours of incubation, the medium was replaced by a fresh culture medium containing resazurin with a final concentration of 0.2 mg/ml, and after a new incubation period of 4 hours, the amount of resorufin fluorescence was determined with excitation at 540 nm and measurement of its emission at 590 nm using the microplate reader. The data obtained was analyzed to calculate the IC50 with GraphPad Prism software.

2.11 *In vitro* relaxivity studies

Samples of Porph(GdDTTA)$_4$ were diluted in injection saline (0.154 M NaCl) to various concentrations of Gd (0, 0.05, 0.1, 0.5 and 1 mM).

In vitro relaxivity experiments were performed by recording T_1 and T_2 maps with a vertical 7T micro MRI imaging spectrometer equipped with an ultra-shielded refrigerated magnet (300WB, Bruker, Avance II, Wissembourg, France), a RF quadrature bird cage coil with an internal diameter of 40 mm (Bruker) and an active shielded gradient channel of 200 mT.m^{-1}. The Paravision 5.1 software enables acquisitions with the following parameters: for T_1 mapping: RARE images; TE

= 13 ms; TR = 15s, 8s, 3s, 1.2s, 0.8s, 0.594s, 0.3s, 0.144s, 0.05s, 0.033s, RARE factor 2; for T_2 mapping: multi-echo MSME images: Hermitian pulse, TR / TE = 15 s / 11 ms, 32 echoes. Fields of view of 3 × 3 cm^2, a matrix size of 128 × 64 and a slice with a thickness of 1.5 mm were used for both mappings.

The relaxation times T_1 and T_2 of each sample were calculated by fitting the intensity of the S-weighted signal T_1 and T_2 with the relation (for T_1: $y = A + B \times (1-\exp(-1 / T_1))$; for T_2: $y = A+B \times \exp(-1/T_2)$.

The molar relaxivities r_1 and r_2 expressed in $mM^{-1}.s^{-1}$ were obtained using the following equation: $1 / T_i = r_i [Gd] + 1 / T_i, 0$ with i: 1 or 2.

2.12 Mouse colon tumor model

A mouse bearing a subcutaneous CT26-Luc tumor[23] for monitoring by bioluminescence imaging of tumor growth, was sacrificed 14 days after implantation. The tumor was removed and immersed in DMEM culture medium and cut into 3 mm^3 fragments.

8-week-old female Balb-C/JRJ mice with a mean weight of 20 g (Janvier, Saint Genest de l'Isle, France) were implanted with a CT26 tumor fragment subcutaneously in both flanks.

The CT26 cell line (ATCC; LGC standards, Molsheim, France) originated from a chemically induced undifferentiated colon carcinoma. After implantation, tumor growth and weight of the mice were monitored daily using a caliper and scale. All work on animals was carried out in accordance with the institutional guidelines of the animal protocol in place at the University of Paris, referral CEEA34 apafis 18.037 and approved by the Ethics Committee No. 34 of the University.

2.13 *In vivo* biodistribution studies by MRI

In vivo biodistribution studies were carried out by MRI to assess uptake, persistence and elimination of the product by the tumor, kidneys, muscle, spleen and liver according to the protocol developed in our facility.[24,23]

Briefly, 8-week-old female BALB / c JRJ tumor bearing mice (Elevage Janvier, France) were anesthetized by inhalation of isoflurane, with respiration and temperature monitoring.[23] 100 µL of the product Porph(GdDTTA)$_4$ in a 0.9 % saline NaCl solution with an optimized concentration of 10 mM in Gd (50 µmol/kg) were injected intravenously via the tail vein through a 30 G catheter, with n = 6 mice for reproducibility.

The images were acquired on the 7 Tesla (300 MHz) microimaging spectrometer (Bruker, Wissembourg France) with image acquisition and processing protocol developed using Paravision 5.1 software previously.[24]

After positioning the anatomical sections recorded in the axial directions to locate the different organs of the mice (T1-weighted FLASH, 23 slices at 1mm, TE / TR 3.5 s/ 500 ms, NA: 4, NR: 1, scan time: 4 - 6 min, flip angle: 80 °, matrix 256 x256, FOV: 3 cm x 3 cm, in plane pixel resolution = 117 µm x 117 µm), 5 sections of 2mm thickness positioned to include the liver, spleen, kidneys, tumors are selected and DCE Dynamic Contrast Enhanced T1-weighted images with Intragate Flash sequences to overcome motion artefacts and DCE T_1-weighted multi-slice sequence images were recorded.

T_1-weighted DCE images were recorded during 40 min including pre and post injection performed 3 min after running a 40 min DCE protocole, and punctual measurements were recorded at 1 h, 3 h, 6 h and 24 h post injection.

The scanning time was of the order of 3 minutes 14 s per image which was sequentially recorded before and after the injection of the agent, Total Scan time: 40min). The acquisition parameters are: (IG FLASH, 5 slices of 2 mm, TR / TE: 100/4 ms, FOV: 3x3 cm, matrix 128x128,, flip angle: 80 °, Time frame: 13, NR: 190, Pixel resolution: 236 µm / pixel dynamic tracking is measured from a first acquisition period of 40 min (13 images), then at 3 h, 6 h, 24 h and 48 h after injection with an IG FLASH acquisition: (IG FLASH, 5 slices of 2 mm, TR / TE: 100/4 ms, FOV: 3x3 cm, matrix 128x128, flip angle: 80 °, Time frame 3.

T_1 maps were recorded at 1h, 3h, 6h and 24h to quantify the Gd content *in vivo* (RAREVTR sequence: Hermitian pulse, flip angle of 90°, TE=11/22/33/44/55/66/88 ms, TR=5/2/1.2/0.8/0.6/0.5/0.25/0.19 s. A field of view of 3 cm×3 cm, a matrix size of 256×128 corresponding to 117 µm×234 µm).

2.14. Protocol for the evaluation of PDT treatment *in vivo*

Balb-C / JRJ mice (female, Elevage Janvier, France) bearing bilateral CT26-Luc tumors on the flank were randomly separated into four groups to provide five mice for each group (n = 5, Table 1).

Group 1: Naive mice;

Group 2: Irradiation : mice not injected with PS and irradiated mono-laterally with a laser at a wavelength of 645 nm (15 min, nominal 20 mW, 100 $mW.cm^{-2}$, 191 $J.cm^{-2}$) 1 hour after injection;

Group 3: PS : mice intravenously injected with PS (50 µmol (Gd).kg^{-1} body weight, 100 µL) and not irradiated;

Group 4: PS_PDT : mice injected with PS (50 µmol (Gd).kg^{-1} body weight, 100 µL) by the intravenous route and irradiated in mono lateral at a wavelength of 660 nm (15 min, nominal 20 mW, 100 mW.cm^{-2}, 191 J.cm^{-2}) 1 hour after injection.

Table 1 : Groups of mice for the *in vivo* evaluation of PDT

	Name	PS	Irradiation
Group 1	Naive	-	-
Group 2	Irradiation	-	+
Group 3	PS	+	-
Group 4	PS_PDT	+	+

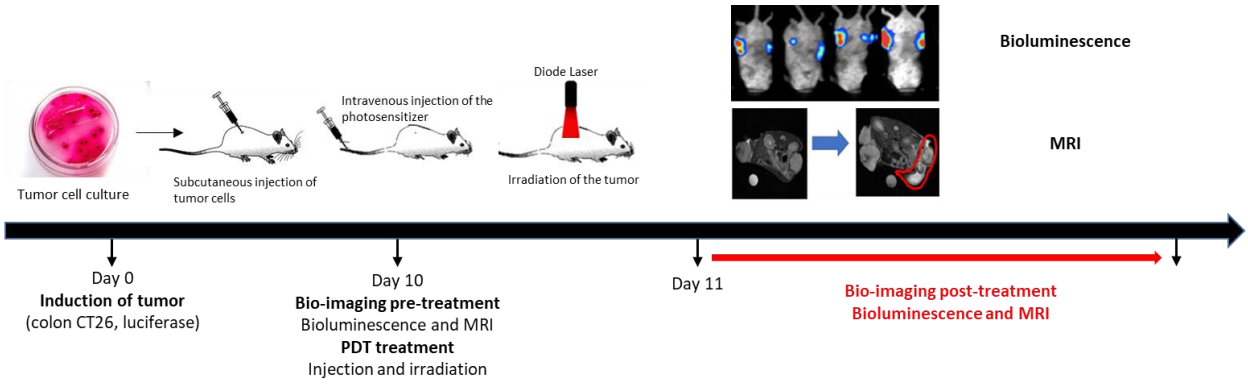

Figure 1 : Timeline scheme of the *in vivo* PDT treatment evaluation.

As depicted in Figure 1, ten days after implantation of the tumor, the photosensitizer was injected intravenously with a catheter (30 G) placed in the tail vein of mice in groups 3 and 4. The mice were anesthetized with 1.5% isoflurane gas in an air / O_2 mixture at 0.5 L/min and 0.2 L/min respectively.

After being anesthetized, the right tumors of mice in groups 2 and 4 were exposed to mono-photon light from a laser fixed in a three-axis holder (coupled fiber diode laser, Qphotonics). Prior to irradiation, the tumor site was disinfected with ethanol. A black mask was placed around the mouse tumor to expose only the tumor to irradiation.

Tumor volume and body weight were measured and recorded daily. The tumor volume was calculated using the following formula: Volume = (Length × $Width^2$) / 2.

2.15 Evaluating the effectiveness of treatment by optical imaging

Luciferin (D-luciferin, Fluoprobes salt K +, Interchim) in the form of potassium salt, diluted in PBS 20 mg/ml was injected ip at 2 mg (100 µl from a 20 mg/ml PBS solution) per mouse, in large excess relative to the quantity of luciferase. Optical imaging was performed with a cooled Intensified Charge Coupled Device (CCD) camera (Biospace, PhotonImager Optima Paris, France). The acquisition of luminescence was initiated 20 min after injection of the substrate with a duration of 10 min. The level of luminescence expressed in ph/s/sr/cm^2 was evaluated by a region of Interest (ROI) applied to the tumor zone (M3 Vision, Biospace software, Paris, France) and the kinetics ratio signal/ D0. The four groups of mice underwent the same protocol before treatment (pre-treatment) and 24 hh, 48 h, 72 h post-treatment.

2.16 Evaluating the effectiveness of PDT treatment by MRI

2.16.1. MRI acquisitions

The images were acquired with a 7 Tesla (300 MHz) microimaging spectrometer (Bruker, Wissembourg, France) as described previously. Mice were anesthetized with 1.5 % isoflurane gas

in air/O_2 75/25 % at 0.2 L/min. The respiratory rate was monitored throughout the procedure as well as the temperature.

To monitor tumor volume and the appearance of necrosis and / or inflammation due to PDT treatment, T2 * and T2 weighted MRI images were acquired before treatment, then 24, 48 and 72 h post-treatment.

The T2 * images are recorded with a FLASH sequence: Hermitian pulse of 2 ms, TR / TE = 350/5 ms, tilt flip angle of 40 °, synchronized with the respiration. A field of view of 3 cm x 3 cm, a matrix size of 256 x 256 corresponding to 117 µm x 117 µm in plane resolution and 19 to 25 slices with a thickness of 1 mm were used, for an acquisition time about 7 min.

T2-weighted images are recorded with the RARE sequence: (TR / TE = 2500/22 ms, 21 slices at 1 mm, RARE factor = 4, scan time: 10 min, Matrix: 256x256, FOV: 3 cm x 3 cm, same slice and in plane resolution as T2*, FLASH images: Hermitian pulse, TR/TE=350/5 ms, flip angle of 40°, triggered on respiration. A field of view of 3 cm ×3 cm, a matrix size of 256×256 corresponding to 117 µm×117 µm).

2.16.2 MRI data analysis

Tumor volume was measured from T_2-weighted images: each slice was opened in ImageJ software (National Institutes of Health, Bethesda) using the BrukerOpener plugin and region of interest (ROI) from the tumor was delimited manually to provide in each slice an area expressed in mm^2. Knowing that the thickness of the slice was 1 mm, the tumor volume was obtained by adding the volume calculated for each slice to provide a final volume in mm^3. The normalized tumor volume was then calculated at each time point by dividing the tumor volume by that of the tumor at D0.

To assess the effectiveness of the treatment and compare the different groups of mice, the percentage under percentile 25 and percentile above 75, respectively %p25 and %Ap75 post-treatment methodology was used[23]. Briefly, the pixel intensity distribution of each tumor was obtained from of T_2-weighted images, the percentage of pixels under the value I0.25 = 0.25 x (Intensitymax -Intensitymin) and the percentage of pixels above the value I0.75 = 0.75 x (Intensitymax -Intensitymin) have was calculated and written %p25, %Ap75 using the Matlab software (cf. SI 9).

The Mann-Whitney non-parametric test was used to compare two by two groups, the values p are obtained.

To measure the Gd concentration in tumors by MRI, during the biodistribution studies, T_1 maps were computed and plotted in function of time. And the derived concentration C were evaluated from the formula : $1/T_i = r_i \times C + 1/T_i°$ i=1,2.

Tumor volume and body weight were measured and recorded daily. Tumor volume was calculated by the following standard formula: Volume = (Length × Width^2) / 2

2.17 Evaluation of treatment efficacy by histology

Following the applied PDT treatment, the 20 mice from a first pool were sacrificed 24 h after the treatment, the tumor was removed and quickly frozen in isopentane cooled with liquid nitrogen. In order to evaluate the ex vivo perfusion of the tumors, mice were injected iv with 100μL of Hoechst 33342 solution (10 mg / kg dissolved in physiological saline, molecular probes, Eugene, OR, USA) 1 min before sacrifice. Hoechst 33342 is a nucleic acid marker that fluoresces blue when bound to dsDNA and is used as marker of *in vivo* functional tumour vasculature.[12]

Ten µm sections of frozen tissue were obtained in the central axial plane of the tumor, placed on histological slides (Polysine®, CML, Nemours, France) and stored frozen at -80 °C. before staining. All stainings were performed at the same time and microscope image scanning was performed under identical lighting conditions to ensure that the analyzes of the different slides were comparable.

2.17.1 Microvascular Density (MVD)

The quantification of vascularization was performed using anti-CD31 (PECAM1) labeling consisting of a three-step procedure as described above[25]. Briefly, tissue sections were first incubated with the primary monoclonal anti-mouse CD31 (PECAM1) monoclonal antibody (BD Biosciences, le Pont de Claix, France; 15.6 μg/mL) for 2 h at 37°C. The slices were then incubated for 30 minutes with the secondary goat anti-rat biotinylated rat secondary antibody (0.5 mg/mL) and finally with streptavidin-conjugated peroxidase (Sigma, 1/400 dilution). Staining was performed with a 3,3-diaminobenzidine substrate (DAB, Sigma) to obtain a brown precipitate. Tissues were counter-stained with Gill hematoxylin to visualize the cell nuclei.

The quantification of the number of vessels per square millimeter (mm^2) was performed on 10 images extracted from the virtual section at x20 magnification recorded on a Olympus microscope and calculated with a home-made specific macro under the ImageJ[26] software as described above.[27]

2.17.2 Cellularity

The quantification of the number of cells was analyzed on the same images using a specific home made macro developed under the ImageJ software, i.e. the contrast was improved (saturation = 50), the background was subtracted (roll = 100 lights), the image was transformed into 8 bits. Then the brightness was adjusted from 69 to 255 and the image was binarized. Finally, a watershed

filter was applied to separate nuclei and particles with a size from 20 to 1000 and a circularity from 0 to 15.

2.17.3 Necrosis

A hematoxylin eosin counterstain was performed for the evaluation of necrosis[10]. Slides were washed with distilled water and fixed for 20 minutes with 4% paraformaldehyde in phosphate buffer. The slides were then cleaned under running water for 5 minutes and stained in hematoxylin solution for 1 minute. Differentiation was performed in saturated lithium solution for 5 min. The slides were then stained with eosin for 30 s. Finally, the slides were dehydrated in alcohol and mounted with Eukitt's fast hardening mounting medium, (Sigma-Aldrich, St. Louis, MO, USA). Necrosis analysis was performed by quantifying the percentage of necrosis in the local areas (center and edges). To obtain a necrosis value at the edge and center of the tumor, a quantification of the number of areas of pink staining per square millimeter (mm^2) was performed in five different selected points on the same slide per animal.

2.17.4 Immune response

Against many pathogens such as viruses or tumor cells, an innate immune response is the first line of defense. A battery of enzymatic biomarkers, antibodies or defense cells are involved in this immune response. Among them, T lymphocytes play an important role and express the membrane marker CD3. Therefore, the detection of this CD3+ T cell marker (IGR Facility, Villejuif, France) was sought in the studied tumors to verify if the immune response was further activated with our theranostic PS. The quantification of CD3 cell density was performed on 10 images recorded on a Zeiss photonic microscope, located in the center (n=5) and in the periphery (n=5) of the tumor with a x20 magnification after a calculation performed with a specific homemade macro under the ImageJ software.

2.17.5 Statistical analyses

The histological result was expressed as mean ± SEM, a unidirectional analysis of variance and the Bonferroni multiple comparison test was applied to determine the significance of the result, P-value Summary: <0.001 Extremely significant ***; 0.001 to 0.01 Very significant **; 0.01 to 0.05 Significant *;> 0.05 Not significant.

3. RESULTS AND DISCUSSION

The synthesis of the theranostic agent Porph(GdDTTA)$_4$ (see Fig 2) that consists of a free base *meso*-tetraarylporphyrin connected to four Gd(III)DTTA complexes (DTTA: diethylenetriamine-N, N, N", N"- tetraacetate) was previously reported,[18] DTTA being a heptadentate ligand, two water molecules complete the coordination sphere of the Gd(III) ion of each complex.

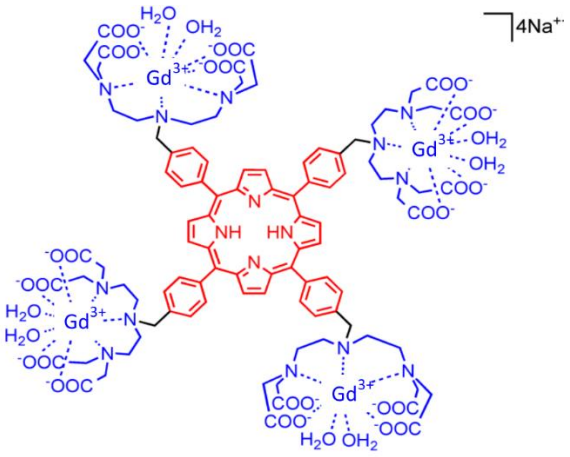

Figure 2: Chemical structure of the theranostic agent Porph(GdDTTA)$_4$.

3.1 Photophysical properties

In previous studies, the water-soluble compound was shown to have the lowest Q absorption band at 634 nm in water adjusted at pH 7. It is capable of generating singlet oxygen with a quantum efficiency of 0.45 in water H_2O at pH 7 and upon irradiation at 516 nm.[18] We evaluated the photophysical properties of this compound with our following experimental conditions. In aqueous D_2O solution, the complex was found to have a luminescence quantum yield of 0.072 and a fluorescence lifetime of 11 ns. The ability to catalytically generate singlet oxygen from molecular oxygen was tested using a direct and indirect method at the irradiation wavelengths 505/510 and 660/670 nm in an air-saturated D_2O solution, with absorbance of 0.2. Singlet oxygen quantum yields of 0.42/0.39 were obtained at 505/510 nm respectively in a D_2O solution with the corresponding methods, which is comparable to the previously reported value (equal to 0.45).[12] Upon irradiation at 660/670 nm, singlet oxygen quantum yields of 0.24/0.28 in a D_2O solution were measured. This again indicates that the compound has an effective photosensitization potential in aqueous solution.

The absorption spectra as a function of time from 1 to 10 min irradiation at 510 nm corresponding to *in vivo* irradiation durations are stable, suggesting a molecular stability of the theranostic compound upon irradiation generating singlet oxygen (see SI2 Fig SI 2), an important characteristic feature for its application *in vivo* as a photosensitizer for PDT.

3.2 Cellular Internalization

In a preliminary study, we found that Porph(GdDTTA)$_4$ internalised in Hela cells.[18] In this present study, we wanted to evaluate its internalization in cancer cells and non-cancerous cell lines. For this purpose, the internalization of the compound was tested in human colon adenocarcinoma

cancer HT-29, murine colon adenocarcinoma CT26 cell lines and non-cancerous human MRC-5 and murine TIB-75 cell lines.

The theranostic agent Porph(GdDTTA)$_4$ seems to accumulate inside the cell after 4 hours (intracellular cytoplasmic compartment) with a higher internalization in HT-29 and CT26 malignant cells compared to healthy MRC-5 and TIB-75 cells, where a very weak or even no fluorescent signal is observed by confocal microscopy (Figure 3). Contrarily to our theranostic agent, the commercial photosensitizer PpIX seems to accumulate efficiently in both tumor and healthy cells, resulting in an apparent specificity of Porph(GdDTTA)$_4$ towards tumor cells, after 4 hours of incubation with the cells. Porphyrins derivatives are known to accumulate selectively in cancer cells[28,29]. This selectivity could be explained by the fact that Porph(GdDTTA)$_4$. is an amphiphilic molecule. It has hydrophilic groups, allowing high solubility, and hydrophobic core, which would facilitate the passage through the membranes. PpIX protoporphyrin is very hydrophobic, which would probably explain its strong affinity with the membranes[30] of the both normal and tumor cells studied in this work and its similar internalization in healthy and tumor cells.

Each PS has its own cellular internalization, localization is governed by its physicochemical characteristics, protein binding capacity, aggregation state, extra and intracellular concentration and incubation time.[31] It has been shown that the mechanisms of uptake may be complex, such as simple diffusion across the lipid bilayer, endocytosis after the hydrophobic association of PS with transportation blood plasma proteins such as LDL[32] and HSA biomolecules.[28]

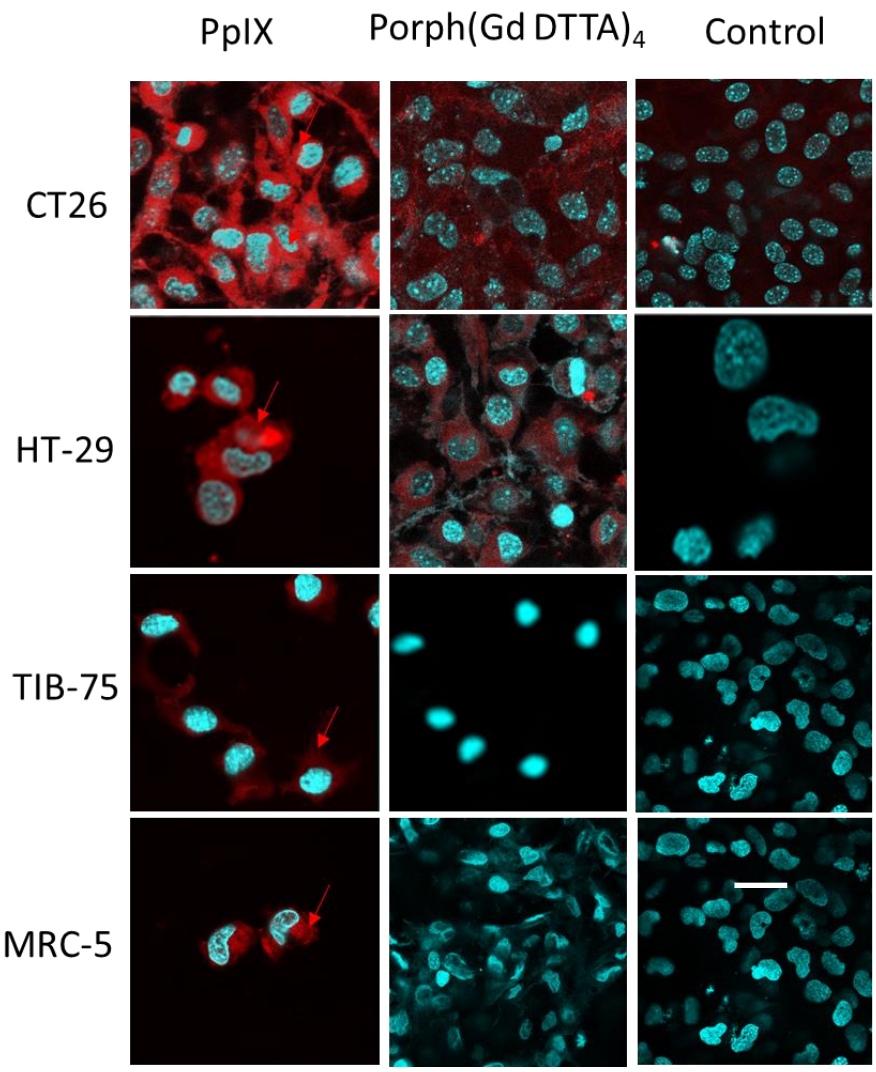

Figure 3: Confocal microscopy images of photosensitizer Porph(GdDTTA)$_4$, PpIX and the control in the absence of PS, in four cell lines. Blue color is the Hoechst nuclei staining, and red color is the porphyrins fluorescence. Red arrows show the fluorescence of the PS after 4 hours incubation at 1 µM.

The dark cytotoxicity of the PS was investigated and evaluated in the same four cell types, namely CT26, HT-29, TIB-75 and MRC-5, after 24 hours of incubation (Table 2, Figure SI 3). A low cytotoxicity of Porph(GdDTTA)$_4$ was evaluated for concentrations below 23 µM with cell viability greater than 90 % (SI 3 Figure SI 3). The concentration of PS necessary to kill 50% of

the cells (IC_{50} values) was determined to be approximately 23 μM for CT26, 84 μM for TIB-75, 334 μM for HT-29 and 98 μM for MRC-5. The values for the dark toxicity of Porph(GdDTTA)$_4$ are close to the range reported for the related free-base porphyrins (~20-85 μM),[33] the IC_{50} value for the gadolinium complexes used for MRI is in the range of mM.[34] This allows to conclude that the photosensitizer Porph(GdDTTA)$_4$ combining the porphyrins and the Gd complex is mildly toxic in the dark and that the PDT studies could be performed safely with concentrations at 10 % of the dark cytotoxicity around 1 μM in vitro.

It is interesting to emphasize that the strongest cytotoxicity is observed on the murine tumor CT26 cell line compared to the non-cancerous cell lines TIB-75 or MRC-5. Concerning the human cells line, the cytotoxicity is more important on the control cell line MRC-5 (IC_{50} value of 98 μM) compared with the malignant cell line HT-29 (IC_{50} value of 334 μM, see table 1 and SI 3, cytotoxicities IC_{50} curves).

Table 2: IC_{50} cytotoxicity assays results of Porph(GdDTTA)$_4$ and PpIX.

IC_{50} (μM) Incubation time 24h	Murine cell lines		Human cell lines	
	Malignant CT26	Reference TIB-75	Malignant HT-29	Healthy MRC-5
Porph(GdDTTA)$_4$	23 ± 3	84 ± 15	334 ± 100	98 ± 17
PpIX	24 ± 3	44.5 ± 0.3	>300	>300

The lower IC_{50} value for CT26 tumor cells is consistent with the apparent stronger selective internalization in these tumor cells, compared to reference TIB-75 or MRC-5 cells. The IC_{50} values

for the dark toxicity of the theranostic agent are close to the values found for PpIX, which are superior to 300 µM for HT-29 and MRC-5, and 24 µM for CT26 and 44.5 µM for TIB-75.

3.3 Phototoxicity

The phototoxicity of Porph(GdDTTA)$_4$ was evaluated on 4 types of cell lines (CT26, HT-29, TIB-75 and MRC-5) incubated for 4 h with a concentration ranging from 0-300 µM and irradiated at 645 nm (10 J.cm^{-2}) for 20 min after washing. The maximum irradiation time of the cells was determined after having irradiated them without PS incubation, at different exposure times to light (cf. Figure SI 4). In order to determine the phototoxicity index (PI), control plates of the different cells were just incubated for 4 hours with the product. Cell viability was determined 48 hours after irradiation (cf figure SI 5). The results are shown in Table 3. The phototoxicity index of Porph(GdDTTA)$_4$ is from 202 and 20 respectively for CT26 and reference TIB-75 cells, and 10 for HT-29 and with IC_{50} superior to 30 for reference MRC-5 cells. (Table 2). The PI of Porph(GdDTTA)$_4$ on murine tumor cells CT26 is ten times higher compared to the healthy reference TIB-75 cells. Likewise, the PI on human tumor HT-29 cells is more than thirty times higher compared to healthy MRC-5 cells.

Table 3 : Porph(GdDTTA)$_4$ phototoxicity assay IC50 and PI.

IC_{50} (µM)	Murine cell lines		Human cell lines	
Incubation time 4 h	CT26	TIB-75	HT-29	MRC-5
Dark	142 ± 12	241 ± 98	> 300	> 300
Light at λexc = 645nm	0.7 ± 0.1	12.0 ± 0.6	30.0 ± 0.2	> 300

PI	202	20	10	undefined

These results are consistent with those obtained in cell internalization studies, where an apparent increased accumulation in tumoral cells is observed. Strikingly, the lead compound of this study was found to be non-toxic in the dark at even higher concentrations (IC_{50}, dark > 300 µM for human cells and > 100 µM for murine cells) compared to the commercially available PpIX (IC_{50}, dark < 100 µM cf. SI 4), while being highly phototoxic in the low micromolar range (IC_{50}, 645 nm = 0.7 ± 0.1 µM for CT26, IC_{50}, 645 nm = 30 ± 0.17 for HT-29) with exceptionally high PI values (PI @645 nm > 200 for CT26, PI @645 nm > 10 for HT-29) more specifically to tumor cells.

It is important to note that under identical experimental conditions, treatment with PpIX showed a strong phototoxic effect for both malignant and non-malignant cell lines (IC_{50} = 0.4-0.7 µM for tumour cells and IC_{50} = 7-10 µM for healthy cells) (SI 6 Table). This result is consistent with the extensive and non-selective internalization of commercial porphyrin in both healthy and tumour cells observed in the cell internalization study by confocal microscopy (Figure 3). The minimal uptake of Porph(GdDTTA)$_4$ for MRC-5 human reference normal cell line indeed compared to tumoral cell lines, contrarily to PpIX molecule could be rationalized by the higher hydrophobicity, asymmetry and hydrophobic membrane permeation of PpIX. Indeed, Nishida et al. (2021)[29], evaluated the intracellular distribution of porphyrin, and show that porphyrin was internalized by endocytosis and direct membrane permeation through the phospholipid bilayer. Similarly to Josefsen et al. (2012)[28], they evidence that it forms very strong hydrophobic π–π stacking interactions with blood proteins in particular albumin, and the porphyrin–protein complexes are selectively taken up by cancer cells, by endocytosis of albumin, the primary pathway for tumor accumulation of porphyrins. Additionally, Mihai et al. (2023)[29] evidenced that asymmetric structure of porphyrin with less bulky substituent was found to favor the internalization by

endocytosis and direct permeation, such as for PpIX. The charges of the porphyrins seem therefore to impact less the cells uptake.

This result shows that the Porph(GdDTTA)$_4$ is more selective to murine tumor cells and able to act at lower drug concentration, with a high PI of 202 compared to a clinically utilized tetrapyrrolic compound (5-ALA precursor of PpIX).

Thus, the PI values of Porph(DTTA)$_4$ are interesting from the perspective to apply and monitor PDT *in vivo*.

3.4 Relaxivity studies in solution

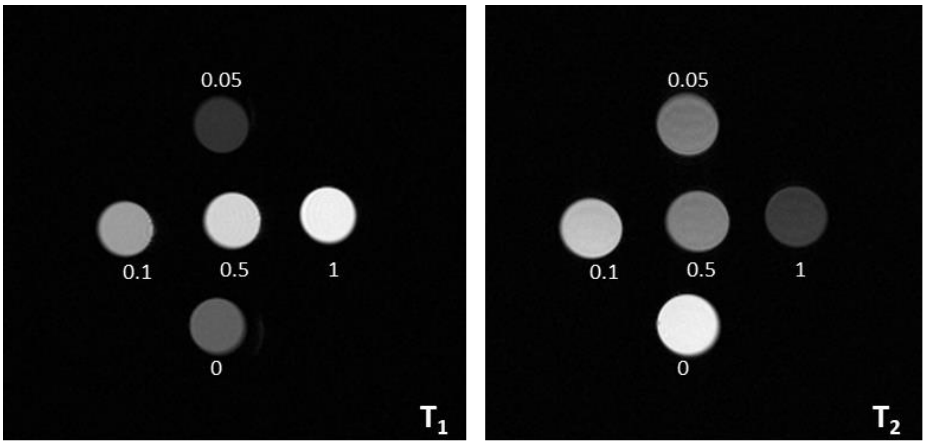

Figure 4: MRI T_1 and T_2 weighted images at 7T of Porph(GdDTTA)$_4$ at various 0, 0.05, 0.1, 0.5 and 1mM Gd^{3+} concentrations in saline (NaCl 154 mM) at 293K.

The T_1 weighted images (Figure 4 T_1) from the PS sample at various Gd concentrations from 0.05 to 1 mM Gd^{3+} visualized strong brightness for the high concentrated samples as expected for T_1 Gd contrast agent. It should be noted that this theranostic molecule provides also T_2 dark signal also on T_2 weighted images, making it possible to be a T_2 contrast agent.

Table 4: r1 and r2 relaxivity values of Porph(GdDTTA)$_4$ and Dotarem® in saline NaCl 0.9% at 7T, 293K.

Porph(GdDTTA)$_4$ $mM^{-1}.s^{-1}$	Dotarem® $mM^{-1}.s^{-1}$
$r_1 = 7.5 \pm 0.8$	$r_1 = 4.1 \pm 0.2$
$r_2 = 68.9 \pm 7.0$	$r_2 = 3.9 \pm 0.2$

The relaxivities of the theranostic compound expressed in Gd concentration were measured in the injection solution from various Gd concentrations (0, 0.05, 0.1, 0.5, 1 mM), at 7T and 293K (Table 4). We recorded values of r_1= 7.5 and r2 = 68.9 $mM^{-1}.s^{-1}$, which is of the same order of magnitude as the r_1 = 8.8 m $mM^{-1}.s^{-1}$ obtained in previous studies in 50 mM NaCl, at 7T, 293K[18] and which are higher values than those of the commercial Dotarem® (r_1= 3.9 and r_2= 4.1 $mM^{-1}.s^{-1}$ at 7T). As previously explained,[18] this relaxivity r_1 increase is related to the two inner-sphere water molecules and to the medium size of the compound, which enables to maximize the relaxivity at high magnetic field. The high r_2 values from magnetic susceptibility effects can be explained by a macromolecular behavior due to the 4 DTTA Gd arms in addition to the π–π stacking which contributes to the aggregation of the porphyrinic moieties in saline at this high mM concentrations which induces a magnetic susceptibility effect as described in the literature.[18,31]

Other porphyrin based molecules of DPP-ZnP-(GdDOTA)$_2$[16] and GdDOTA-ZnP-ZnP-GdDOTA[17] complexes consisting of π-extended Zn(II) porphyrin linked to two GdDOTA-type complexes for magnetic resonance imaging (MRI) detection were developed as photosensitizers for PDT. Both molecules showed high relaxivity per Gd ions (r1= 19.32 $mM^{-1}s^{-1}$ and 14.33 mM^{-1} s^{-1}, for DPP-ZnP-(GdDOTA)$_2$ and GdDOTA-ZnP-ZnP-GdDOTA respectively, at 20 MHz and 298 K) compared to clinical contrast agents at this low magnetic field. *In vitro* Hela cells studies

of internalisation and *in vitro* PDT at 660 nm evidenced also the potentiality of these molecules as theranostic agent.

3.5 Biodistributions studies *in vivo* by MRI.

The visual semi-quantitative analysis of the *in vivo* biodistribution of the Porph(GdDTTA)$_4$ measured by dynamic MRI shows a clear enhancement of the signal in the MR image (Figure 5 a) into the tumor areas at 30 minutes with a maximum intensity around 40 minutes, a remanence at more than 50 % of the MRI intensity of and a clearance time superior to 24 h. The DCE profile into the kidney shows similar pharmacokinetic behavior with a lower signal enhancement as regard to the tumor.

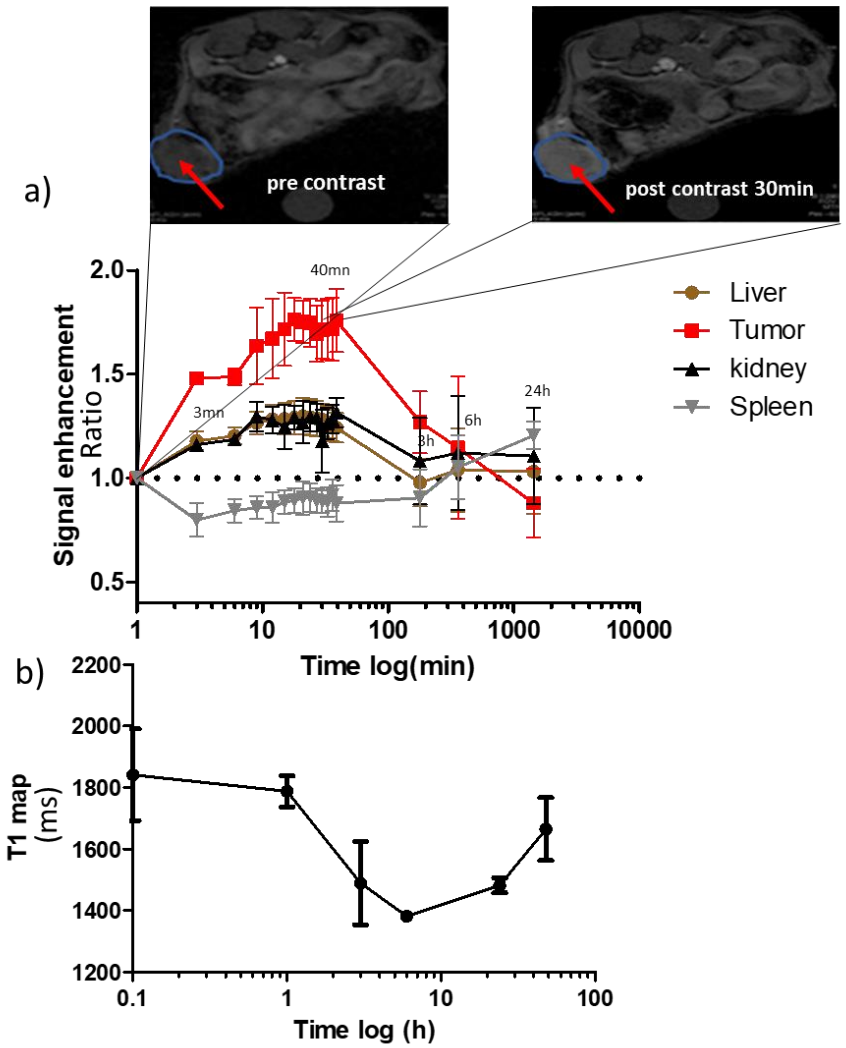

Figure 5: Biodistribution studies *in vivo* of Porph(GdDTTA)4 by a) DCE Dynamic Contrast Enhanced MRI on tumoral Balbc/JRJ mice n=6 (red arrows : tumor) and b) corresponding quantitative T_1 map in tumor to measure the amount of Gd CA.

The quantitative T_1 map (Figure 5 b) is related to the computed concentrations evolution in time ($1/T_1$ proportional to the CA concentration, with the hypothesis of $r_1 \sim r_1$ in saline physiological solution) into the tumor more accurately than the DCE T_1 weighted method and confirms the

dynamic biodistribution profile of the PS with a maximum uptake at about 40 min and a 24 h remanence duration (Fig SI 8).

Figure 5 a shows MRI cross-sections where the tumoral regions are highlighted as expected for the biodistribution of objects with size inferior to 5 nm. Comparison of the pre-contrast and post-contrast MR images clearly reveals the higher brightness of the kidney and liver caused by Porph(GdDTTA)$_4$ (see the Supplementary Information Fig. SI 7). The peaks of enhancement were observed at the same time, 3 minutes post-injection for all CA in the liver and the kidney followed by a phase of decay (Fig 5 a. and SI 7). The absolute values at 40 min post injection are the highest signal for the PS in the time profile (see red arrow, +75 % in the tumor, and fig 7a + 25 % in the liver, 10 % in the cortical region of the kidney), suggesting this best timing window for PDT irradiation.

The CA are excreted from the liver and from the kidney cortex via the bladder as expected considering the molecular weight of the molecule M = 2.6 kD, size smaller than 30-50 kD, 5 nm. After 24 h, the levels of Porph(GdDTTA)$_4$ came back to their 20 % of the pre-contrast values, for tumor and kidney, liver, related to their clearance.

These *in vivo* results underline the benefit of this molecular theranostic agent to optimize the PDT protocol based on MR imaging. This imaging study indicates that this Porph(GdDTTA)$_4$ displays higher contrast enhancements over the full time period observed with detectable imaging properties, with a remanence window around 40-60 min (Table 5).

In addition, this mid-size molecular moiety is advantageously eliminated after 24 h from all the organs, preventing the undesired long liver uptake of several days observed usually for nanoparticles. This kinetic renal elimination rather than the liver route indicates also a molecular biological behavior rather than a nanoparticular long time liver clearance[35]. The charges of this

porphyrin ensure its solubility in biological medium as shown by the biodistribution in many organs (liver, kidney, and tumor), and the molecular size would rather drive the kinetic biodistribution.

Table 5 : Capture, maximum, remanence and clearance timings of the theranostic photosensitizer evaluated *in vivo* by MRI.

Organ	Beginning of capture (min)	Maximum capture time (min)	Remanence time at signal >+50 % (h)	Clearance time (h)
Tumor	3	40	6	>24
Kidney	3	40	6	>24
Liver	3	18	3	6
Spleen	9	18	3	6

Concentration of Gd 1 h post contrast can be calculated from the formulae: Concentration = $(1/T_1° - 1/T_1) / r1$ with the hypothesis of similar relaxivities values r1 in tissue as in physiological solutions. (cf Fig SI 8). The quantitative results of T_1 mapping, which provide a measurement of Gd concentrations and thus of the theranostic agent, shows the optimized presence of the photosensitizer in the tumor during 3 h and confirms the results obtained in qualitative biodistribution by T_1-weighted DCE sequences.

The theranostic PS showed an MRI signal enhancement (Table 5) 3 min after injection, a maximum at 40 min post-injection, and a high retention of about 3-6 h till about 24 h, which presents a sufficient time interval for the application of PDT irradiation. For comparison in the

literature, Magnevist [Gd(III) complex of DTPA], a standard MRI agent that clinicians used in routine presents a shorter 0.2 hours half-life in blood, and half-life of elimination of 1.6 hours.[27]

Compared with the few theranostic agents in the literature, our results are in coherence. Goswami et al.[12] synthesized a HPPH-aminobenzyl-Gd(III)-DTPA (3-(1′-hexyloxyethyl) pyropheophorbide-a (HPPH) containing 3 Gd(III) aminophenyl DTPA) in particular, and recorded an enhancement of the MRI signal during 8 h post-injection, which reflects a long circulation in the blood. Yuzhakova et al.[36] observed on their two photosensitizers of gadolinium (III) cations chelated by tetrapyrrolic macrocycles (GdPz1 and GdPz2) a remanence of more than 3h post injection in CT26 tumors *in vivo*.

Notably, the quicker elimination of our studied PS from the bloodstream with a 20 % remaining MRI signal post 24 hours will help reducing side effects associated with sunlight exposure.[29]

3.6 Application of PDT treatment

With our compounds in hand, the next step was to assess the *in vivo* activity of the theranostic PS. For this purpose, twenty female 7 weeks old Balb-C mice bearing CT26 tumors (Elevage Janvier, France) were randomly separated into four groups, resulting in five mice for each group, Group 1 : Naïve, Group 2 : Irradiation, Group 3 : PS, Group 4 : PS_PDT. Ten days after tumor implantation, the PS was injected with 100 µl at 10 mM Gd intravenously with a catheter (30 G) placed in the tail vein for groups 3,4. Mice were anesthetized with 1.5% isoflurane gas in an air/0_2 mixture at 0.5 L/min and 0.2 L/min respectively.

3.7.1 Monitoring the efficacy of PDT by bioluminescence and MRI imaging

A :

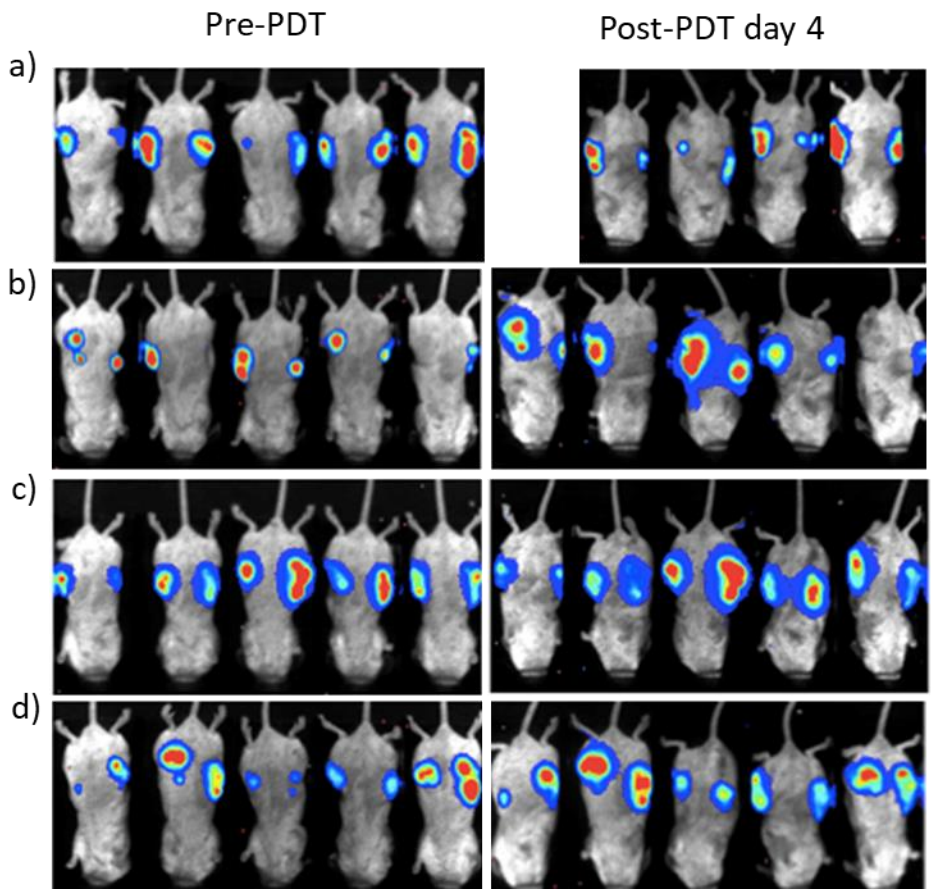

a) Group 4 PS_PDT b) Group 1 Naive c) Group 2 Irradiation d) Group 3 PS

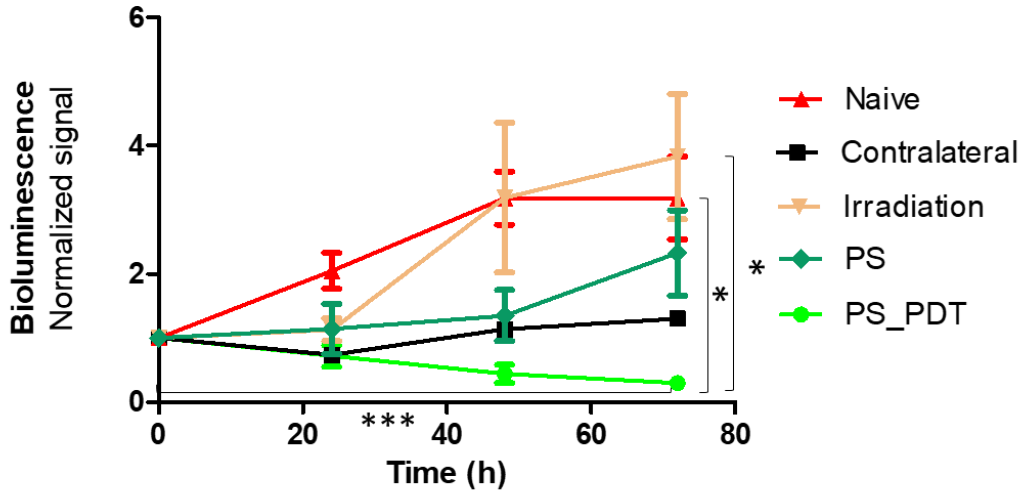

B :

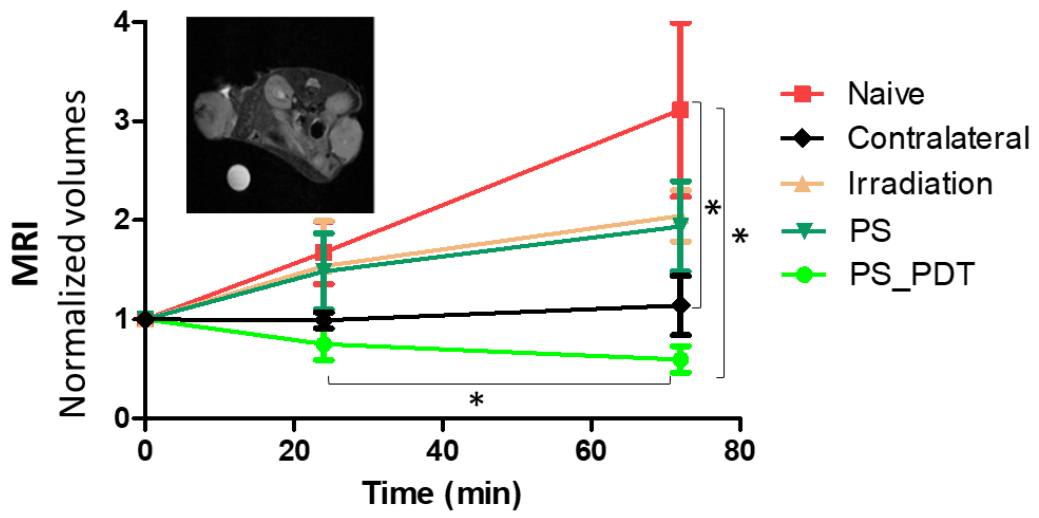

Figure 6: *In vivo* bioimaging for tumor growth study after PDT. A : Bioluminescence normalized signal evolution (measured in ph/cm^2/s/sr) of the CT26 tumor mice 24h, 48, 72 h post PDT. a) PS_PDT: PS + irradiation, b) Naïve, c) Irradiation alone, d) PS alone. B : MRI tumor volume growth measured at 0, 24 h, 72 h . Mann-Whitney test, n=5, *P<0.05

In order to evaluate the tumor burden (activities), we measured the bioluminescence signal related to the tumor at 24, 48 and 72 h post full PDT with Porph(GdDTTA)$_4$ molecule injection and irradiation normalized to the injection day as shown in Figure 6 A. The result shows that PDT significantly decreases the tumor burden at day 4 post PDT compared to control mice naïve mice. For the group PS_PDT (PS + irradiation), we observed a significant impact of the tumor activity during 72 h post irradiation, while for the group of mice that received the injection of the photosensitizer only or irradiation only, a stabilization of the bioluminescent signal in function of time was observed compared to the group of naive mice. It should be noted that contralateral PDT (no irradiation of the tumor) tumor shows a tendency to stabilise, suggesting an immune effect as described in the literature.[1]

The tumor growth was also quantified by 3D MRI which provides a more accurate real 3D volume of the tumor. Figure 6 B.

3.6.2 Monitoring the effectiveness of PDT by MRI imaging

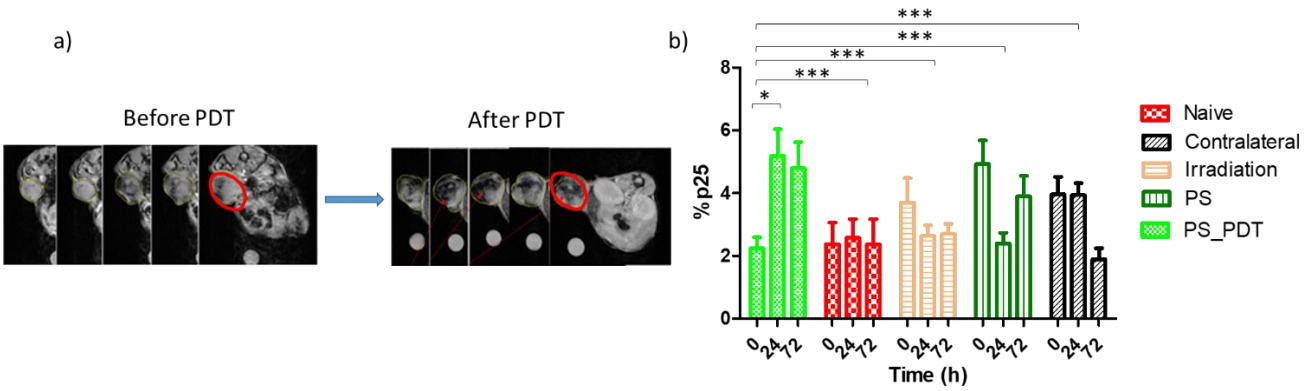

Figure 7: Necrosis detection by *in vivo* MRI induced by PDT. (a) MRI images before and after PDT. (b) percentile %p25 graphs at 0, 24 and 72 h post injection.

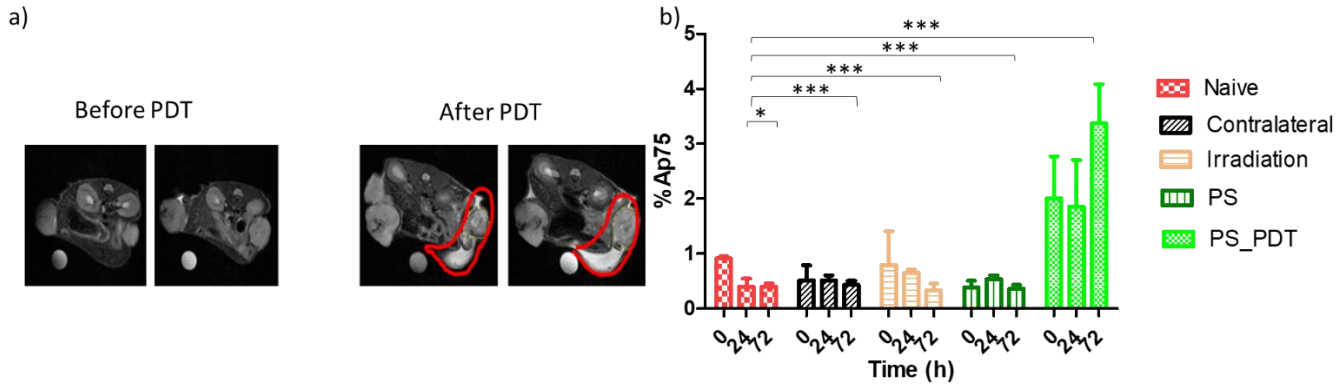

Figure 8: Inflammation induced by PDT visualized by *in vivo* MRI a) MRI images before and after PDT. (b) percentile %Ap75 graphs at 0, 24 and 72 h post injection.

The monitoring the effectiveness of PDT by MRI imaging was assessed by using a post-processing methodology previously described with a new parameter %Ap0.75 (% Above percentile 75 %, cf SI 9) computing bright intensity pixels attributed to inflammation by MRI.

The %p0.25 and %Ap0.75 in the treated tumor was significantly higher compared to the control groups (Figures 7 and 8, respectively). 24 h after injection of the theranostic agent and irradiation, the %p0.25 and %Ap0.75 significantly increased reflecting the necrosis and inflammation respectively which are the expected consequence of the treatment PDT. Our hypothesis is that the irradiation of the tumor after injection the theranostic photosensitizer induced the photoactivation of the photosensitizer and after expected ROS release, tumor cells die, leading to tumor volume impairment.

Optical bioluminescence imaging becomes a widely non-invasive, low cost, user friendly, and quantitative imaging modality reflecting the malignant biological activity reported by the luciferase gene expression in tumoral cells. However, the bioluminescence signal could be affected by ATP[37] and O_2 level.[38] To improve the accuracy of tumor growth impacted by PDT, the effect of the therapy was evaluated by measurements of tumor volume growth by MRI (Figure 6 B) as MRI modality provides absolute accurate and quantitative 3D volume measurement. At 24 h after treatment, we observe that the complete theranostic treatment with irradiation shows a significant decrease with a significant tumor regression observed at 24 h post treatment compared to naïve group. Furthermore, longitudinal follow-up describes a decrease in tumor volume with a significant difference still present 4 days after this complete PDT treatment. The contralateral tumor shows a mild non-significant tumor development compared to the control tumors of the "naive" tumor bearing mice. This slowing down of a non-irradiated contralateral tumor is known

in the literature and could be explained by the development of an immune effect[1,39] remaining to be further investigated. Overall, we have therefore provided proof of concept of the efficacy of the treatment strategy with this novel theranostic PS.

This result confirms our MRI observations in the follow-up of tumour growth assessment by bioluminescence imaging.

Compared with the theranostic MRI porphyrins in the literature, the Gd-DTPA-porphyrin conjugate of Hindré *et al*. showed high magnetic contrast in vitro, cell internalisation by fluorescence microscopy and generation of singlet O_2 in solution.[11] TPP-Gd_2(DTPA)$_4$[12], HPPH-3GdDTPA[13] and Gd_4DTTA porphyrin complex[15] derivatives show also high relaxivities and similar PDT *in vivo* efficacy in tumor in the red region, 650-680 nm. A Zn phthalocyanine conjugated with GdDO3A-amide complex[40] showed good photophysical and photochemical properties *in vitro*, as well as high MR contrast agent feature to generate a potential theranostic PDT agent. Porphyrazines functionalized with GdDO3A-amide such as ZnPz-nGd (n = 1, 2, 4, 8)[14], showed a high relaxivity at 60 MHz, 30 times higher for the n=8 complex, than the mono GdDO3A, a good internalization in cells compared with clinical PS, kept electronic spectroscopic features as non-functionalized Zn-porphyrazine and demonstrated efficient PDT in vitro. One of the complex Gd (ZnPz-1Gd) provided efficient PDT *in vivo*.

Yuzhakova et al.[36] used this same *in vitro* and *in vivo* evaluation strategy for the study of 2 theranostic porphyrazines GdPz1 and GdPz2. By fluorescence imaging *in vivo*, the group observed a notable signal by fluorescence, and up to 96 h with a greater accumulation at 24 h in tumoral tissues compared to other tissues: skin, abdomen, lungs. By MRI at 9.4 T, they observed a remanence of more than 3 h. The r_1 relaxivities were lower than the one of the commercial agent Dotarem®, whereas the r2 relaxivities measured by this team are extremely high, due to the PS

interaction with the solubilisation polymers. Indeed, pre-solubilisation of these agents in a 5% PEG polyimide solution was necessary. PDT treatment of CT26 tumors with one of the GdPz1 agents had no impact on their growth, while the second GdPz2 agent caused moderate inhibition of tumor growth, with more pronounced differences from untreated tumors at day 21 after tumor inoculation (11 days after treatment). The authors quantified *in vitro* higher phototoxicity index (PI) for the GdPz2 (PI about 10 times higher than for GdPz1) which could explain the PDT efficiency of only the second PS. Different experimental parameters such as different internalization, dose used, fluence (100 mW/cm^2, 120 J/cm^2) and irradiation wavelength at 600 nm lower than our 640 nm wavelength, the 3h post injection irradiation with lower tumor uptake compared to tumor blood higher concentration could explain their moderate impact in PDT efficiency.

Li et al.[13] also evaluated up to the *in vivo* stage their theranostic photosensitiser, HPPH-aminobenzyl-Gd(III)-DTPA produced a remarkable increase in MRI signal 8 hours after iv injection and significant tumoricidal activity, 50 % tumour regression measured by caliper with 80 % tumor disappearance in mice after 90 days.

Further developments of theranostics comprising porphyrinic photosensitizer for PDT and MRI are towards nanotheranostics with for example Iron oxide nanoparticles[41] combining MRI and PDT, and with additional therapy such as CDT[42].

So overall, we have demonstrated the proof of concept of the treatment strategy using this theranostic photosensitizer $Porph(GdDTTA)_4$.

Further complementary experiments using histology were also performed to investigate the microscopic cellular behavior for PDT.

3.8 Histological studies

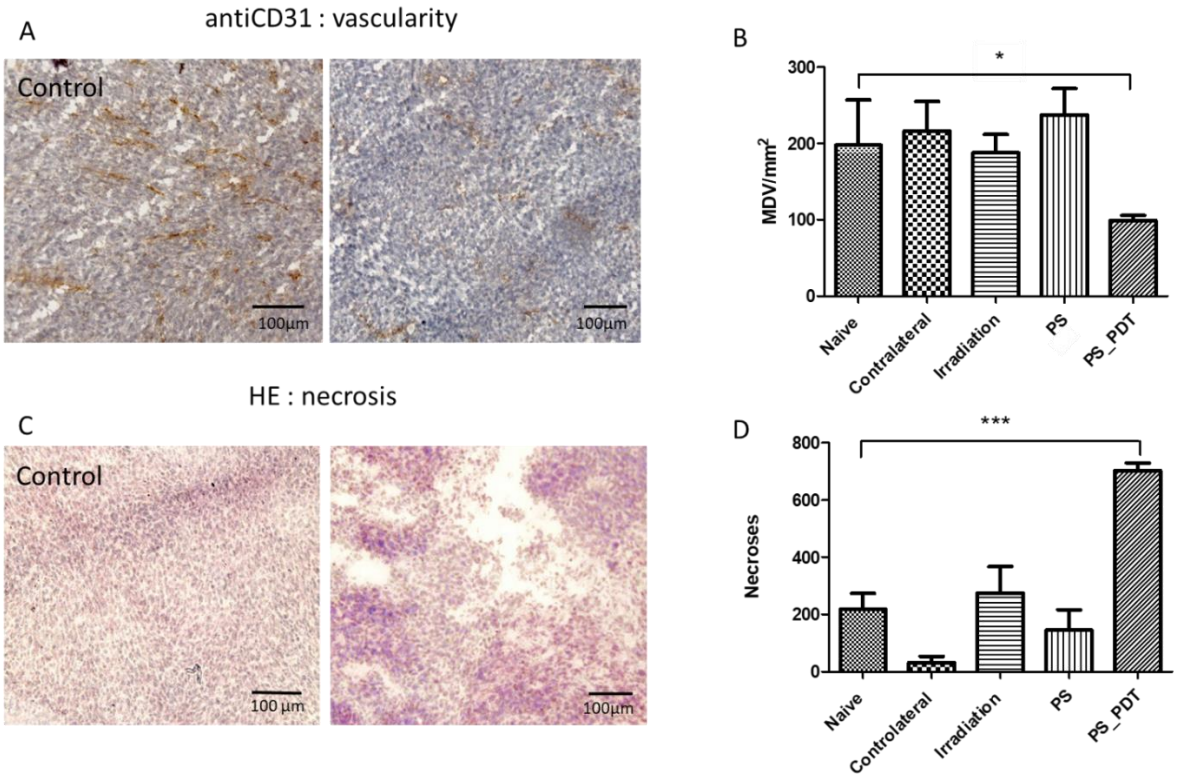

Figure 9 : Histology results, A : images of vascularization and B : graphs of microvascular density (number of vessels pixels/mm^2), C : images and D : graphs of necroses (areas without cells/total area), 1 day after PDT treatment. Mean ± SEM, One way Anova with Dunnett's Multiple Comparison Test, *, p≤.05; **, p≤.01; ***, p≤.001.

In order to confirm these MRI and bioluminescence observations, histological analyses of the tumors were performed for the experimental condition 24 h after treatment. Histological staining of the vascularization (CD31, H Fig 9 A) and the necroses (HE Fig 9 C) was undertaken. Figure 9 presents the results obtained in terms of microvascular density (Fig. 9 B, MVD, number of vessels

pixels/mm^2) and necroses (Fig. 9 D, areas without cells/total area). In Fig. 9 B, the decrease of the MVD for the PDT treatment was significant compared to the control groups. Furthermore, in Fig. 9 D, a significant increase of necrosis was observed also for PDT treatment compared to the controls groups, which are in agreement with the results obtained by MRI.

In order to analyze the 24 h post-treatment environment related to immune response, lymphocytes infiltration via the expressed biomarker CD3 was analyzed by immunohistochemistry and quantification was performed using a macro programmed in Image J software dedicated to the segmentation of histological parameters based on contrast and color.

We observed a significant increase in CD3 cell density on treated tumors compared to naive mice (Figure 10). A non-significant increase on the only irradiated tumor and on the contralateral tumors of the treated mice which may explain the bioluminescence results and the volume measurement by MRI. For the tumors of the mice receiving only the product, there was no difference in the density of CD3.

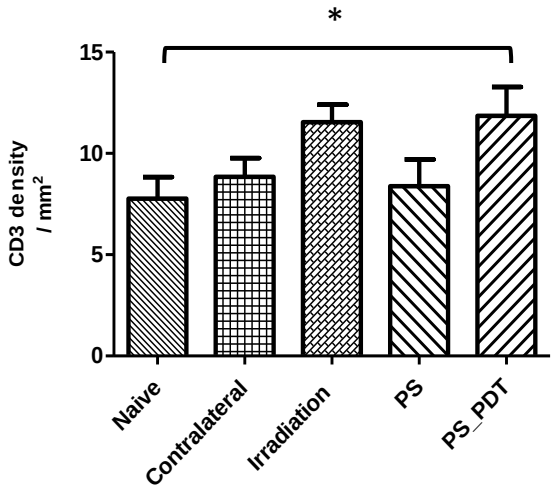

Figure 10 : Quantification of lymphocytes density within the irradiated tumor and the contralateral tumor. Mann-Whitney test, n=5, *p<0.05.

These results show the presence of a localized immune effect at the level of the PDT treatment, but no significant immune CD3 effect on the other contralateral tumor.

Some preclinical studies in different animal models demonstrate that in addition to the direct cellular and vascular effect, PDT shows proinflammatory effects capable of inducing an anti-tumor immune response.[43,1]

Recent evidence has also suggested that PDT-induced vessel occlusion, ischemia, and direct tumor cell killing lead to a significant local inflammatory response.[1,44] The photo-oxidative degradation of membrane lipids and the production of metabolites caused by necrosis are important mediators of inflammation.[44] This damage generates various alarm signals (production of inflammatory mediators) that are detected by innate immunity.[31] With the release of histamine and serotonin from the damaged vessels, there is an infiltration of the tumor by various populations of immune cells (lymphocytes and phagocytes).

Vascular damage and tumor necrosis were observed in our PDT experiments and should therefore as observed in the literature described above, induce the activation of inflammatory mediators[32] which could explain the inflammation observed in MRI.

4. CONCLUSION

We propose here to combine therapy with imaging for tumor treatment using a theranostic agent with three abilities of PDT treatment, optical *in vitro* imaging and MRI *in vivo* monitoring. This theranostic agent contains a porphyrin core for the PDT, and optical imaging, functionalized with four gadolinium complexes for MRI detection in order to ensure this dual features. The design of this molecule was made to provide high MRI relaxivity, good stability and solubility in water, an

excitation wavelength at 640 nm near the NIR region in order to increase the penetration of light irradiation in living tissue.

Only the full combination of the photosensitizer administration with irradiation provided a significant decrease of the activity of the tumor cells and tumor volume on *in vivo* tumor model. This was shown 24 h post therapy after one single treatment. This proof of concept is highly interesting as it shows that theranostic agent without irradiation, or irradiation alone are not efficient in inhibiting tumor growth, and with non apparent toxicity *in vitro* and *in vivo*. MRI bioimaging evidenced two aspects: the first one is to be able to follow the biodistribution of the theranostic photosensitizer and the second interest is to evaluate the efficiency of this molecule *in vivo* by showing an increase of the necrosis and inflammation as well as the reduction of tumor size. The efficiency of this PDT treatment was also demonstrated by bioluminescence imaging and histology studies have rationalized the results at the cellular level by showing reduction of the vascularization and increased necrosis.

In the design of innovative theranostic moiety, we have demonstrated that our all-in-one system offers a means of obtaining high-resolution and reproducible MRI images, for the *in vivo* monitoring of therapy, quantitative and accurate follow-up of biological responses and may be an interesting approach for improved biomedical imaging.[8,41,42,45]

It confirms that the perspective of theranostics in routine healthcare to become plausible as an important element of personalized and predictive medicine.[28,46]

ACKNOWLEDGMENT

The Ecole Doctorale ED 406 of PSL/Sorbonne University is thanked for financially supporting SB for her PhD thesis. *In vivo* imagings were performed at the LIOPA UTCBS bioimaging facility

from Life Imaging Facility of University Paris Cité (Plateformes Imageries du Vivant – PIV) and ENSCP, Université PSL. The CD3 labeling was performed by Olivia Bawa, in the PETRA department (Experimental and Translational Pathology) B2M team, at the Institut Gustave Roussy IGR, Villejuif. The confocal imaging experiments were performed at the Plateforme d'Imagerie Cellulaire of the Faculté de Pharmacie, PICMO, UMS 25, Université de Paris Cité. The GDR AIM CNRS is also acknowledged as well as the CNRS, Inserm and ENSCP Chimie Paristech.

AUTHOR INFORMATION

Corresponding Author

*Bich-Thuy DOAN ENSCP Chimie ParisTech, Université PSL, CNRS, UMR 8040, Institute of Chemistry for Life and Health Sciences (I-CLeHS), SEISAD, 11 rue Pierre et Marie Curie, Paris, France; Email : bich-thuy.doan@chimieparistech.psl.eu

Author Contributions

The manuscript was written through contributions of all authors. All authors have given approval to the final version of the manuscript.

Funding Sources

This work was also financially supported by an ERC Consolidator Grant PhotoMedMet to G.G. (GA 681679), has received support under the program "Investissements d'Avenir" launched by the French Government and implemented by the ANR with the reference ANR-10-IDEX-0001-02 PSL (G.G.). LSAMM thanks the icFRC (http://www.icfrc.fr) and LabEx-CSC for financial support.

ABBREVIATIONS

MRI, Magnetic Resonance Imaging; DCE; Dynamic Contrast Enhanced sequence; PS; Photosensitizer, PDT; Photodynamic Therapy; Gd DTTA; Gd diethylenetriamine-N, N, N'', N''-tetraacetate.

ASSOCIATED CONTENT

Supporting Information.

Singlet oxygen measurement methods; Absorption spectra of the theranostic molecule for photostability assay after irradiation at 510 nm; IC_{50} cytotoxicity assays of Porph(GdDTTA)$_4$ in different cell lines; Cell viability for the determination of maximum irradiation time of cells @645 nm without the PS preserving any cells damages with cellular viability superior to 90 %; Phototoxicity IC_{50} graphs of Porph(GdDTTA)$_4$; Phototoxicity results for reference PpIX; MRI images *in vivo* into the liver and the kidney during the DCE dynamic experiment; Concentration dynamic profile evolution within the tumor measured by T_1 map *in vivo* : Calculation of the percentile %p25 and %Ap75 of the MRI images to analyze the necrosis and the inflammation induced by PDT using a home-made Matlab programme.

REFERENCES

(1) Castano, A. P.; Mroz, P.; Hamblin, M. R. Photodynamic Therapy and Anti-Tumour Immunity. *Nat. Rev. Cancer* **2006**, *6* (7), 535–545. https://doi.org/10.1038/nrc1894.

(2) Dougherty, T. J.; Gomer, C. J.; Henderson, B. W.; Jori, G.; Kessel, D.; Korbelik, M.; Moan, J.; Peng, Q. Photodynamic Therapy. *J. Natl. Cancer Inst.* **1998**, *90* (12), 889–905. https://doi.org/10.1093/jnci/90.12.889.

(3) Baskaran, R.; Lee, J.; Yang, S.-G. Clinical Development of Photodynamic Agents and Therapeutic Applications. *Biomater. Res.* **2018**, *22* (1), 25. https://doi.org/10.1186/s40824-018-0140-z.

(4) Lan, M.; Zhao, S.; Liu, W.; Lee, C.-S.; Zhang, W.; Wang, P. Photosensitizers for Photodynamic Therapy. *Adv. Healthc. Mater.* **2019**, *8* (13), 1900132. https://doi.org/10.1002/adhm.201900132.

(5) Ethirajan, M.; Chen, Y.; Joshi, P.; Pandey, R. K. The Role of Porphyrin Chemistry in Tumor Imaging and Photodynamic Therapy. *Chem. Soc. Rev.* **2010**, *40* (1), 340–362. https://doi.org/10.1039/B915149B.
(6) Wachter, E.; Heidary, D. K.; Howerton, B. S.; Parkin, S.; Glazer, E. C. Light-Activated Ruthenium Complexes Photobind DNA and Are Cytotoxic in the Photodynamic Therapy Window. *Chem. Commun.* **2012**, *48* (77), 9649–9651. https://doi.org/10.1039/C2CC33359G.
(7) Heinemann, F.; Karges, J.; Gasser, G. Critical Overview of the Use of Ru(II) Polypyridyl Complexes as Photosensitizers in One-Photon and Two-Photon Photodynamic Therapy. *Acc. Chem. Res.* **2017**, *50* (11), 2727–2736. https://doi.org/10.1021/acs.accounts.7b00180.
(8) Wang, L.-S.; Chuang, M.-C.; Ho, J.-A. A. Nanotheranostics--a Review of Recent Publications. *Int. J. Nanomedicine* **2012**, *7*, 4679–4695. https://doi.org/10.2147/IJN.S33065.
(9) O'Connor, A. E.; Gallagher, W. M.; Byrne, A. T. Porphyrin and Nonporphyrin Photosensitizers in Oncology: Preclinical and Clinical Advances in Photodynamic Therapy. *Photochem. Photobiol.* **2009**, *85* (5), 1053–1074. https://doi.org/10.1111/j.1751-1097.2009.00585.x.
(10) Uthaman, S.; Huh, K. M.; Park, I. K. Tumor Microenvironment-Responsive Nanoparticles for Cancer Theragnostic Applications. *Biomater. Res.* **2018**, *22* (1), 1–11. https://doi.org/10.1186/s40824-018-0132-z.
(11) Hindré, F.; Plouzennec, M. L.; de Certaines, J. D.; Foultier, M. T.; Patrice, T.; Simonneaux, G. Tetra-p-Aminophenylporphyrin Conjugated with Gd-DTPA: Tumor-Specific Contrast Agent for MR Imaging. *J. Magn. Reson. Imaging* **1993**, *3* (1), 59–65. https://doi.org/10.1002/jmri.1880030111.
(12) Goswami, L. N.; White, W. H. I.; Spernyak, J. A.; Ethirajan, M.; Chen, Y.; Missert, J. R.; Morgan, J.; Mazurchuk, R.; Pandey, R. K. Synthesis of Tumor-Avid Photosensitizer−Gd(III)DTPA Conjugates: Impact of the Number of Gadolinium Units in T1/T2 Relaxivity, Intracellular Localization, and Photosensitizing Efficacy. *Bioconjug. Chem.* **2010**, *21* (5), 816–827. https://doi.org/10.1021/bc9005305.
(13) Li, G.; Slansky, A.; Dobhal, M. P.; Goswami, L. N.; Graham, A.; Chen, Y.; Kanter, P.; Alberico, R. A.; Spernyak, J.; Morgan, J.; Mazurchuk, R.; Oseroff, A.; Grossman, Z.; Pandey, R. K. Chlorophyll-a Analogues Conjugated with Aminobenzyl-DTPA as Potential Bifunctional Agents for Magnetic Resonance Imaging and Photodynamic Therapy. *Bioconjug. Chem.* **2005**, *16* (1), 32–42. https://doi.org/10.1021/bc049807x.
(14) Song, Y.; Zong, H.; Trivedi, E. R.; Vesper, B. J.; Waters, E. A.; Barrett, A. G. M.; Radosevich, J. A.; Hoffman, B. M.; Meade, T. J. Synthesis and Characterization of New Porphyrazine-Gd(III) Conjugates as Multimodal MR Contrast Agents. *Bioconjug. Chem.* **2010**, *21*, 2267–2275. https://doi.org/10.1021/bc1002828.
(15) Luo, J.; Chen, L.-F.; Hu, P.; Chen, Z.-N. Tetranuclear Gadolinium(III) Porphyrin Complex as a Theranostic Agent for Multimodal Imaging and Photodynamic Therapy. *Inorg. Chem.* **2014**, *53* (8), 4184–4191. https://doi.org/10.1021/ic500238s.
(16) Jenni, S.; Bolze, F.; Bonnet, C. S.; Pallier, A.; Sour, A.; Tóth, É.; Ventura, B.; Heitz, V. Synthesis and In Vitro Studies of a Gd(DOTA)-Porphyrin Conjugate for Combined MRI and Photodynamic Treatment. *Inorg. Chem.* **2020**, *59* (19), 14389–14398. https://doi.org/10.1021/acs.inorgchem.0c02189.
(17) Schmitt, J.; Jenni, S.; Sour, A.; Heitz, V.; Bolze, F.; Pallier, A.; Bonnet, C. S.; Tóth, É.; Ventura, B. A Porphyrin Dimer-GdDOTA Conjugate as a Theranostic Agent for One- and Two-Photon Photodynamic Therapy and MRI. *Bioconjug. Chem.* **2018**, *29* (11), 3726–3738. https://doi.org/10.1021/acs.bioconjchem.8b00634.
(18) Sour, A.; Jenni, S.; Ortí-Suárez, A.; Schmitt, J.; Heitz, V.; Bolze, F.; Loureiro de Sousa, P.; Po, C.; Bonnet, C. S.; Pallier, A.; Tóth, É.; Ventura, B. Four Gadolinium(III) Complexes Appended to a Porphyrin: A Water-Soluble Molecular Theranostic Agent with Remarkable Relaxivity Suited for

MRI Tracking of the Photosensitizer. *Inorg. Chem.* **2016**, *55* (9), 4545–4554. https://doi.org/10.1021/acs.inorgchem.6b00381.
(19) Karges, J.; Kuang, S.; Maschietto, F.; Blacque, O.; Ciofini, I.; Chao, H.; Gasser, G. Rationally Designed Ruthenium Complexes for 1- and 2-Photon Photodynamic Therapy. *Nat. Commun.* **2020**, *11* (1), 1–13. https://doi.org/10.1038/s41467-020-16993-0.
(20) Nakamaru, K. Solvent Effect on the Nonradiative Deactivation of the Excited State of Tris(2,2'-Bipyridyl)Ruthenium(II) Ion. *Bull. Chem. Soc. Jpn.* **1982**, *55* (5), 1639–1640. https://doi.org/10.1246/bcsj.55.1639.
(21) Karges, J.; Basu, U.; Blacque, O.; Chao, H.; Gasser, G. Polymeric Encapsulation of Novel Homoleptic Bis(Dipyrrinato) Zinc(II) Complexes with Long Lifetimes for Applications as Photodynamic Therapy Photosensitisers. *Angew. Chem. Int. Ed.* **2019**, *58* (40), 14334–14340. https://doi.org/10.1002/anie.201907856.
(22) Kochevar, I. E.; Redmond, R. W. Photosensitized Production of Singlet Oxygen. *Methods Enzymol.* **2000**, *319*, 20–28. https://doi.org/10.1016/s0076-6879(00)19004-4.
(23) Thébault, C. J.; Ramniceanu, G.; Boumati, S.; Michel, A.; Seguin, J.; Larrat, B.; Mignet, N.; Ménager, C.; Doan, B.-T. Theranostic MRI Liposomes for Magnetic Targeting and Ultrasound Triggered Release of the Antivascular CA4P. *J. Controlled Release* **2020**, *322*, 137–148. https://doi.org/10.1016/j.jconrel.2020.03.003.
(24) Fredy, J. W.; Scelle, J.; Ramniceanu, G.; Doan, B.-T.; Bonnet, C. S.; Tóth, É.; Ménand, M.; Sollogoub, M.; Vives, G.; Hasenknopf, B. Mechanostereoselective One-Pot Synthesis of Functionalized Head-to-Head Cyclodextrin [3]Rotaxanes and Their Application as Magnetic Resonance Imaging Contrast Agents. *Org. Lett.* **2017**, *19* (5), 1136–1139. https://doi.org/10.1021/acs.orglett.7b00153.
(25) Seguin, J.; Mignet, N.; Latorre Ossa, H.; Tanter, M.; Gennisson, J. L. Evaluation of Antivascular Combretastatin A4 P Efficacy Using Supersonic Shear Imaging Technique of Ectopic Colon Carcinoma CT26. *Ultrasound Med. Biol.* **2017**, *43* (10), 2352–2361. https://doi.org/10.1016/j.ultrasmedbio.2017.05.013.
(26) Moreno, N. Appendix 4 Image Processing. *Image Rochester N* **2007**, 249–258.
(27) Seguin, J.; Doan, B.-T.; Latorre Ossa, H.; Jugé, L.; Gennisson, J.-L.; Tanter, M.; Scherman, D.; Chabot, G. G.; Mignet, N. Evaluation of Nonradiative Clinical Imaging Techniques for the Longitudinal Assessment of Tumour Growth in Murine CT26 Colon Carcinoma. *Int. J. Mol. Imaging* **2013**, *2013*, 1–13. https://doi.org/10.1155/2013/983534.
(28) Josefsen, L. B.; Boyle, R. W. Unique Diagnostic and Therapeutic Roles of Porphyrins and Phthalocyanines in Photodynamic Therapy, Imaging and Theranostics. *Theranostics* **2012**, *2* (9), 916–966. https://doi.org/10.7150/thno.4571.
(29) Nishida, K.; Tojo, T.; Kondo, T.; Yuasa, M. Evaluation of the Correlation between Porphyrin Accumulation in Cancer Cells and Functional Positions for Application as a Drug Carrier. *Sci. Rep.* **2021**, *11* (1), 2046. https://doi.org/10.1038/s41598-021-81725-3.
(30) Ricchelli, F. Photophysical Properties of Porphyrins in Biological Membranes. *J. Photochem. Photobiol. B* **1995**, *29* (2–3), 109–118. https://doi.org/10.1016/1011-1344(95)07155-U.
(31) Ball, D. J.; Mayhew, S.; Wood, S. R.; Griffiths, J.; Vernon, D. I.; Brown, S. B. A Comparative Study of the Cellular Uptake and Photodynamic Efficacy of Three Novel Zinc Phthalocyanines of Differing Charge. *Photochem. Photobiol.* **1999**, *69* (3), 390–396. https://doi.org/10.1111/j.1751-1097.1999.tb03303.x.
(32) Mojzisova, H.; Bonneau, S.; Vever-Bizet, C.; Brault, D. Cellular Uptake and Subcellular Distribution of Chlorin E6 as Functions of PH and Interactions with Membranes and Lipoproteins. *Biochim. Biophys. Acta BBA - Biomembr.* **2007**, *1768* (11), 2748–2756. https://doi.org/10.1016/j.bbamem.2007.07.002.

(33) Antoni, P. M.; Naik, A.; Albert, I.; Rubbiani, R.; Gupta, S.; Ruiz-Sanchez, P.; Munikorn, P.; Mateos, J. M.; Luginbuehl, V.; Thamyongkit, P.; Ziegler, U.; Gasser, G.; Jeschke, G.; Spingler, B. (Metallo)Porphyrins as Potent Phototoxic Anti-Cancer Agents after Irradiation with Red Light. *Chem. – Eur. J.* **2015**, *21* (3), 1179–1183. https://doi.org/10.1002/chem.201405470.
(34) Siew, E. L.; Farris, A. F.; Rashid, N.; Chan, K. M.; Rajab, N. F. In Vitro Toxicological Assessment of Gadolinium (III) Chloride in V79–4 Fibroblasts. *Genes Environ.* **2020**, *42*, 22. https://doi.org/10.1186/s41021-020-00161-3.
(35) Kobayashi, H.; Brechbiel, M. W. Nano-Sized MRI Contrast Agents with Dendrimer Cores. *Adv. Drug Deliv. Rev.* **2005**, *57* (15), 2271–2286. https://doi.org/10.1016/j.addr.2005.09.016.
(36) Yuzhakova, D. V.; Lermontova, S. A.; Grigoryev, I. S.; Muravieva, M. S.; Gavrina, A. I.; Shirmanova, M. V.; Balalaeva, I. V.; Klapshina, L. G.; Zagaynova, E. V. In Vivo Multimodal Tumor Imaging and Photodynamic Therapy with Novel Theranostic Agents Based on the Porphyrazine Framework-Chelated Gadolinium (III) Cation. *Biochim. Biophys. Acta BBA - Gen. Subj.* **2017**, *1861* (12), 3120–3130. https://doi.org/10.1016/j.bbagen.2017.09.004.
(37) Yeh, H.-W.; Wu, T.; Chen, M.; Ai, H. Identification of Factors Complicating Bioluminescence Imaging. *Biochemistry* **2019**, *58* (12), 1689–1697. https://doi.org/10.1021/acs.biochem.8b01303.
(38) Lambrechts, D.; Roeffaers, M.; Goossens, K.; Hofkens, J.; Putte, T. V. de; Schrooten, J.; Oosterwyck, H. V. A Causal Relation between Bioluminescence and Oxygen to Quantify the Cell Niche. *PLOS ONE* **2014**, *9* (5), e97572. 1-11. https://doi.org/10.1371/journal.pone.0097572.
(39) Mroz, P.; Szokalska, A.; Wu, M. X.; Hamblin, M. R. Photodynamic Therapy of Tumors Can Lead to Development of Systemic Antigen-Specific Immune Response. *PLOS ONE* **2010**, *5* (12), e15194. 1-11. https://doi.org/10.1371/journal.pone.0015194.
(40) Aydın Tekdaş, D.; Garifullin, R.; Şentürk, B.; Zorlu, Y.; Gundogdu, U.; Atalar, E.; Tekinay, A. B.; Chernonosov, A. A.; Yerli, Y.; Dumoulin, F.; Guler, M. O.; Ahsen, V.; Gürek, A. G. Design of a Gd-DOTA-Phthalocyanine Conjugate Combining MRI Contrast Imaging and Photosensitization Properties as a Potential Molecular Theranostic. *Photochem. Photobiol.* **2014**, *90* (6), 1376–1386. https://doi.org/10.1111/php.12332.
(41) Yan, L.; Luo, L.; Amirshaghaghi, A.; Miller, J.; Meng, C.; You, T.; Busch, T. M.; Tsourkas, A.; Cheng, Z. Dextran-Benzoporphyrin Derivative (BPD) Coated Superparamagnetic Iron Oxide Nanoparticle (SPION) Micelles for T2-Weighted Magnetic Resonance Imaging and Photodynamic Therapy. *Bioconjug. Chem.* **2019**. https://doi.org/10.1021/acs.bioconjchem.9b00676.
(42) Jibin, K.; Victor, M.; Saranya, G.; Santhakumar, H.; Murali, V.; Maiti, K. K.; Jayasree, R. S. Nanohybrids of Magnetically Intercalated Optical Metamaterials for Magnetic Resonance/Raman Imaging and In Situ Chemodynamic/Photothermal Therapy. *ACS Appl. Bio Mater.* **2021**. https://doi.org/10.1021/acsabm.1c00510.
(43) Mroz, P.; Szokalska, A.; Wu, M. X.; Hamblin, M. R. Photodynamic Therapy of Tumors Can Lead to Development of Systemic Antigen-Specific Immune Response. *PLoS ONE* **2010**, *5* (12). https://doi.org/10.1371/journal.pone.0015194.
(44) Pizova K, Tomankova K, Daskova A, Binder S, Bajgar R, K. H. Photodynamic Therapy for Enhancing Antitumour Immunity. *Biomed Pap Med Fac Univ Palacky Olomouc Czech Repub* **2012**, *156*, 93–102. https://doi.org/dx.doi.org/10.5507/bp.2012.056.
(45) Luk, B. T.; Zhang, L. Current Advances in Polymer-Based Nanotheranostics for Cancer Treatment and Diagnosis. *ACS Appl. Mater. Interfaces* **2014**, *6* (24), 21859–21873. https://doi.org/10.1021/am5036225.
(46) Park, K.; Lee, S.; Kang, E.; Kim, K.; Choi, K.; Kwon, I. C. New Generation of Multifunctional Nanoparticles for Cancer Imaging and Therapy. *Adv. Funct. Mater.* **2009**, *19* (10), 1553–1566. https://doi.org/10.1002/adfm.200801655.